

3422

Carderock Division
Naval Surface Warfare Center

Bethesda, Md. 20084-5000

CARDIVNSWC-TR-85-94/03 January 1994
Survivability, Structures, and Materials Directorate
Technical Report

**Shipboard Smoke Detection with
Optical Fiber Technology**

by
Henry K. Whitesel, John K. Overby, and David J. Kocsik
Carderock Division, Naval Surface Warfare Center

Richard O. Claus
Virginia Tech

Michael J. Ransford
ECO, Inc.

19980422 143

DTIC QUALITY INSPECTED 4



Approved for public release; distribution is unlimited.

CARDIVNSWC-TR-85-94/03 Shipboard Smoke Detection with Optical Fiber Technology

CONTENTS

| | |
|--|-----------|
| FIGURES | iii |
| TABLES | iv |
| ADMINISTRATIVE INFORMATION | v |
| ACKNOWLEDGEMENTS | v |
| ABSTRACT | 1 |
| INTRODUCTION | 1 |
| EXISTING SENSORS FOR DAMAGE CONTROL SYSTEMS IN THE US NAVY | 2 |
| SMOKE DETECTION REQUIREMENTS FOR FUTURE DC SYSTEMS | 3 |
| PHYSICAL PROPERTIES OF SMOKE | 5 |
| STATE OF THE ART OF SMOKE DETECTORS | 7 |
| IONIZATION SMOKE DETECTORS | 7 |
| PHOTOELECTRIC SMOKE DETECTORS | 8 |
| SMOKE DETECTOR PERFORMANCE COMPARISON | 8 |
| OPTICAL FIBER SMOKE SENSOR DESIGN | 11 |
| OBSCURATION OPTICAL FIBER SMOKE SENSORS | 12 |
| SCATTERING OPTICAL FIBER SMOKE SENSORS | 14 |
| SPECTROMETRIC OPTICAL FIBER SMOKE SENSORS | 16 |
| FLUORESCENCE OPTICAL FIBER SMOKE SENSORS | 20 |
| COMMERCIALLY AVAILABLE OPTICAL FIBER SMOKE DETECTORS | 21 |
| SUMMARY | 21 |
| REFERENCES | 22 |
| APPENDIX A - ANALYSIS OF LIGHT SCATTERING BY SMOKE FOR FIBEROPTIC SMOKE DETECTOR DESIGN | A-1 |
| APPENDIX B - OPTICAL FIBER SMOKE SENSOR TESTS ON EX-USS SHADWELL ... | B-1 |
| INITIAL DISTRIBUTION | Last Page |

FIGURES

| | |
|---|------|
| Figure 1 - Simplified Block Diagram of a Damage Control System. | 2 |
| Figure 2 - Particle Size Distribution for Lamp Wick and Heptane Smokes. | 6 |
| Figure 3 - Operating Principle of an Ionization Chamber Smoke Detector. | 8 |
| Figure 4 - Light Scattering Optics for a Photoelectric Smoke Detector | 9 |
| Figure 5 - Detector Sensitivity for Ionization and Light Scattering Smoke Sensors. | 10 |
| Figure 6 - Optical Fiber Sensor, General Schematic for Damage Control Monitoring | 11 |
| Figure 7 - Obscuration Optical Fiber Smoke Sensor Schematic. | 13 |
| Figure 8 - Scattering Optical Fiber Smoke Sensor Schematic | 15 |
| Figure 9 - Scattering Optical Fiber Smoke Sensor Schematic Using Large Collecting Lens . . | 17 |
| Figure 10 - Schematic Diagram for a Spectrometric Optical Fiber Smoke Sensor | 18 |
| Figure A1 - Geometry of Circular Housing of Fiber-Based Smoke Detector. | A-8 |
| Figure A2 - Algebraic (solid line) and Log-normal (dotted line) Distributions. | A-10 |
| Figure A3 - Digitized Intensity Coefficient $I(q)$ Showing the Polynomial Curve Fit (solid line) and the Gaussian Curve Fit (dotted line) to the Data (circles) | A-13 |
| Figure A4 - Scattered Intensity for a Single Incident Ray | A-14 |
| Figure A5 - Total Scattered Intensity for each Ray Interacting with a Smoke Particle | A-15 |
| Figure A6 - Scattered Intensity for a Single, Gaussian Distributed, Incident Ray. | A-16 |
| Figure A7 - Total Scattered Intensity for each Gaussian Distributed Ray Interacting with a Smoke Particle | A-17 |
| Figure B1 - Second Deck Plan View, Ex-USS SHADWELL. | B-2 |
| Figure B2 - Third Deck Plan View, Ex-USS SHADWELL. | B-3 |
| Figure B3 - Spectrometric Optical Fiber Smoke Sensor Element | B-4 |
| Figure B4 - Spectrometric Optical Fiber Smoke Sensor Opto-electronics Package. | B-4 |
| Figure B5 - Optical Fiber Smoke Sensor Test Results Ex-USS SHADWELL Fire Test FD_F19 Sept 1993 | B-5 |

| | |
|--|------|
| Figure B6 - Optical Fiber Smoke Sensor Test Results Ex-USS SHADWELL Fire Test FD_D1 Sept 1993 | B-6 |
| Figure B7 - Optical Fiber Smoke Sensor Test Results Ex-USS SHADWELL Fire Test FD_F7 May 1993. | B-7 |
| Figure B8 - Optical Fiber Smoke Sensor Test Results Ex-USS SHADWELL Fire Test FD_F6 April 1993 | B-8 |
| Figure B9 - Optical Fiber Smoke Sensor Temperature Test at 30 Percent Relative Humidity, 08 Nov 1993. | B-10 |
| Figure B10 - Optical Fiber Smoke Sensor Humidity Test at 30 Degrees C, 09 Nov 1993 .. | B-11 |

TABLES

| | |
|--|---|
| Table I - Performance Goals for Damage Control Smoke Sensors. | 4 |
|--|---|

ADMINISTRATIVE INFORMATION

This work was sponsored by the Naval Research Laboratory as Task 4 of the Damage Control Project of the Surface Ship Technology Program, Program Element 62121N, Block NDIA, Project Number RH21S22. The Damage Control Project is managed by Dr. Patricia Tatem of the Naval Research Laboratory. The Surface Technology Program is managed by Daniel Winegrad of the Naval Surface Warfare Center, Carderock Division, and sponsored by James Gagorik of the Office of Naval Research.

ACKNOWLEDGEMENTS

Dr. Patricia Tatem of the Naval Research Laboratory provided program guidance for this work and took an active interest during the course of this development; her interest is greatly appreciated. The program support of Mr. Daniel Winegrad of the Naval Surface Warfare Center, Carderock Division, and the financial support of Mr. James Gagorik of the Office of Naval Research is also greatly appreciated.

Henry Whitesel is the primary author of this report and functioned as the project manager and principle engineer on this task. John Overby made all the equipment work and provided many creative development ideas and solutions to unexpected problems. Rick Claus analyzed the scattering properties of smoke and Mike Ransford experimented with the scattering sensors. David Kocsik drew most of the illustrations.

SHIPBOARD SMOKE DETECTION WITH OPTICAL FIBER TECHNOLOGY

ABSTRACT

Reliable smoke detectors are needed on Navy ships to detect and characterize fires for input to damage control systems. Optical fiber technology offers a potential opportunity to improve the state of the art of smoke detectors by reducing false alarms, improving reliability, and providing continuous measurement of visibility in each ship compartment. The objective of this work is to assist in developing fire fighting strategy and damage control on Navy ships to improve operational and combat readiness. Optical fiber smoke sensor designs depend on the measurement of optical power absorption (obscuration) and scattering across an air gap. Utilizing spectrographic techniques and dual detector designs potentially compensates for optical power changes, ambient light changes, dirt coatings, and water coatings; sensing the types of smoke particles present is also possible, and is desirable as this leads to identification of types of fires. Designs of optical fiber smoke sensors were completed, were tested successfully on the ex-USS SHADWELL, and are ready for transition to 6.3 programs or to industry. Using multiplexing and multimode technology should reduce the unit measurement cost to values acceptable to the Navy and the industrial market.

INTRODUCTION

The Navy is developing new optical fiber sensors to detect and characterize shipboard fires. This report documents the development and application of optical fiber smoke detectors as fire detectors; it is a follow-on report to one previously issued on the development and application of optical fiber temperature sensors as fire detectors.^{1,2} The detection and measurement of smoke density will improve the ability of surface ships to absorb damage and continue fighting. A complete shipboard fire detection system might utilize temperature, smoke, flame, and combustion sensors.

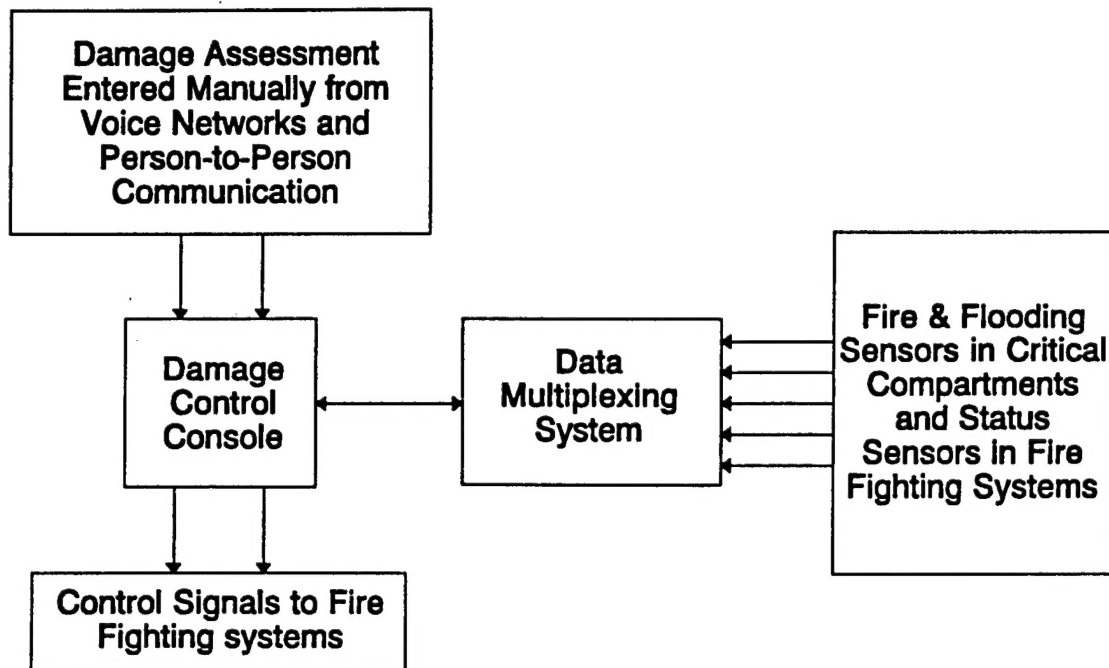
Goals of the damage control development project are to develop systems that will determine the damage condition of surface combatants in near real time (less than 3 seconds after the event) and will make recommendations to the damage control officer that will aid in controlling ship damage. In general, meeting these goals requires sensors that are installed in every compartment, indicate the location and severity of the damage, and that have the ability to survive shipboard fires. Optical fiber technology provides the opportunity for designing damage control sensors to meet these performance goals. When fully developed, optical fiber sensors have significant advantages such as reduced electromagnetic interference (EMI), smaller size and weight, faster time response, improved reliability, ease of networking the increased number of sensors required to monitor every compartment, and, in some cases, reduced cost.

This report reviews the state of the art of smoke sensor design, using both electrical and optical approaches and identifies methods of improving the smoke sensor design using optical fiber technology. Theoretical analysis backed up with experimental results from hardware designs are the basis for results presented herein.

EXISTING SENSORS FOR DAMAGE CONTROL SYSTEMS IN THE US NAVY

Damage control system design is different for each class of Navy ships depending on the mission of the ship and the state of the technology at the time of ship design. Figure 1 illustrates the Navy's most advanced damage control monitoring system design in simplified form; it is close to the DDG-51 baseline design.

Figure 1 - Simplified Block Diagram of a Damage Control System.



The sensors are threshold detectors for fire and flooding of critical compartments, and status of the fire fighting systems. Outputs of the sensors are transmitted through the data multiplexing system for analysis and display at the damage control console (DCC). Damage assessment can also be manually entered into the DCC; information is gathered from the voice communications networks and from person-to-person discussions. Some valves and pumps in the fire fighting systems are activated from the DCC.

The original baseline design for the DDG-51 included about 70 flooding alarm sensors and over 200 fire/smoke alarm sensors. Improvements to that design for the Flight 2A class could increase the fire/flooding sensor populations to about 90 flooding alarms, and 650 fire/smoke alarms (with the preponderance in the smoke category, but also adding about 50 flame detectors).

New shipboard systems, presently in development, that will provide improvement to the methods of controlling shipboard damage are the Integrated Survivability Management System

(ISMS), the Battle Damage Assessment System (BDAS), and the Standard Monitoring and Control System (SMCS). These new system designs provide improved methods of transmitting, analyzing, and displaying damage control information; no sensor improvements are specifically planned at the present time. The new system designs will vastly improve the time of response to damage situations but may not realize their full potential unless sensor improvement programs are established and executed.

Ionization smoke detectors are used for fire detection in the DDG-51 baseline design and all previous ship designs; they sound an alarm and transmit a signal when the smoke obscuration exceeds a threshold set between 0.5 and 4 percent per foot, for gray smoke. Photo-electric smoke detectors are usually not used onboard ship.

SMOKE DETECTION REQUIREMENTS FOR FUTURE DC SYSTEMS

Smoke sensing requirements were estimated from the damage control system performance requirements established for the 6.2 damage control project. To fully meet the system design goals, the smoke sensors must be continuously indicating, instead of alarms, and should be sufficiently inexpensive to be installed in every compartment on the ship. At the beginning of this development program, all the activities in the Navy damage control community were surveyed to determine quantitative smoke sensor requirements. Table I lists the resulting performance goals of smoke sensors for damage control monitoring. (Note these are performance goals; the 6.2 program results only in developing the measurement methodology. To fully meet these goals a follow on Advanced Development Program is required.)

The rationale for some of these specifications originates in the system architecture and conceptual design. Comprehensive monitoring for smoke in all ship's compartments is required to diagnose damage conditions in the desired 3 seconds. The sensor elements and connecting cable will be designed to survive all but the hottest fires. The opto-electronics packages will be a low temperature design and therefore will have to be duplicated to ensure maintaining monitoring capability in every compartment in the event of one casualty. In Table I, there are two input ranges listed for smoke density. One is for a fire detection mode and the other is for a visibility measurement mode at high smoke densities. Fire fighters would like to know the visibility in a space prior to entering. These smoke sensors will require little or no maintenance except for occasional calibration.* Smoke density measurement to 538°C (1000°F) was not demonstrated during this effort but is thought not to be a problem; high temperature performance is likely a matter of proper material selection and packaging.

a) Another program involving the development of self calibrating optical fiber sensors will significantly reduce the calibration time making it feasible to keep maintain thousands of shipboard sensors, without using massive amounts of man power. Reference, Whitesel, Henry K., Gordon W. Day, Allen H. Rose, and Catherine A. Miller, Self Calibrating Optical fiber Sensors: Potential Design Methods, Carderock Division Naval Surface Warfare Center Technical Report CARDIVNSWC-TR-80-92/15, May 1993.

Table I - Performance Goals for Damage Control Smoke Sensors.

| PARAMETER | PERFORMANCE GOALS |
|---|---|
| Input Range | Detection mode: 0% to 9% per foot obscuration for both gray and black smoke. Visibility Mode; 0% to 100% per foot obscuration. |
| Accuracy | ±0.5% per foot obscuration |
| Resolution | ±0.1% per foot obscuration |
| Desired Unit Production Cost (per measurement) | <\$200 |
| Size | <20 cubic inches |
| Weight | <1 pound |
| Output Signal | 4-20 ma, 0-10 vdc, or digital for DMS, FODMS, or SAFENET |
| Response Time | <3 seconds |
| Mean Time Between Failure | >100,000 hours |
| Mean Time Between False Alarms | <1 per 50,000 hours |
| Mean Time To Repair | <1 hour |
| Operating Life | 40 years |
| Environmental Temperature | Sensing Element and Cable: 0°C to 538°C (32°F to 1000°F) Opto-electronics: 0°C to 65°C (32°F to 149°F) |
| Environmental Relative Humidity | 0% to 100% |
| Environmental Vibration | MIL-STD-461, Level I |
| Environmental Shock | MIL-STD-901 |
| Environmental Atmosphere | Salt Spray and dust |
| Input Power | < 100 milliwatts per sensor (115VAC, 60 Hz) |
| Calibration | Self Calibration daily |
| Special Considerations: All optical parts conform to NAVSEA military standards, and every compartment has a smoke sensor. | |

In general, smoke sensors trigger an audio or electrical alarm when an adjustable threshold of obscuration is exceeded; the threshold is set between 0.5 and 4 percent per foot (for gray smoke) depending on the cleanliness condition of the space being monitored. For most threshold type smoke detectors, including the photoelectric, ionization chambers, and the optical fiber types disclosed in this report, a continuous measurement of obscuration is intrinsically done in the sensor; it is a small expense to actually use that information that is already present. The continuous (or analog) information is very useful because it can be used by the sensor network processing to help diagnose the origin and location of the fire. The pattern of smoke density will likely diffuse upward and outward from the origin compartment, depending on the status of the hatch and door closures and the ventilation system status. If smoke sensors are developed to have a visibility mode that measures obscuration over the 0 to 50 percent per foot range, this information can be used to help develop fire fighting strategy and to control smoke removal systems.

PHYSICAL PROPERTIES OF SMOKE

Smoke is composed of particulate and gaseous matter given off by fires. Smoke detectors use the particulate part of smoke as the measurand. Obscuration is an optical property of smoke that is primarily related to particle concentration or smoke density. The problem of designing smoke detectors is very much tied to how smoke detectors are specified and the properties of the smoke particulate in terms of particle size and distribution. Smoke detectors are specified to measure obscuration.

The definition of obscuration is based on a test developed by Underwriters Laboratories.³ Light is produced by a tungsten filament automotive lamp, driven with a constant current source, and is transmitted across a 1.5 meter (5 feet) air gap. Received light is detected with a barrier type selenium photovoltaic cell enclosed in a hermetically sealed case. At any air gap distance, the obscuration will be:³

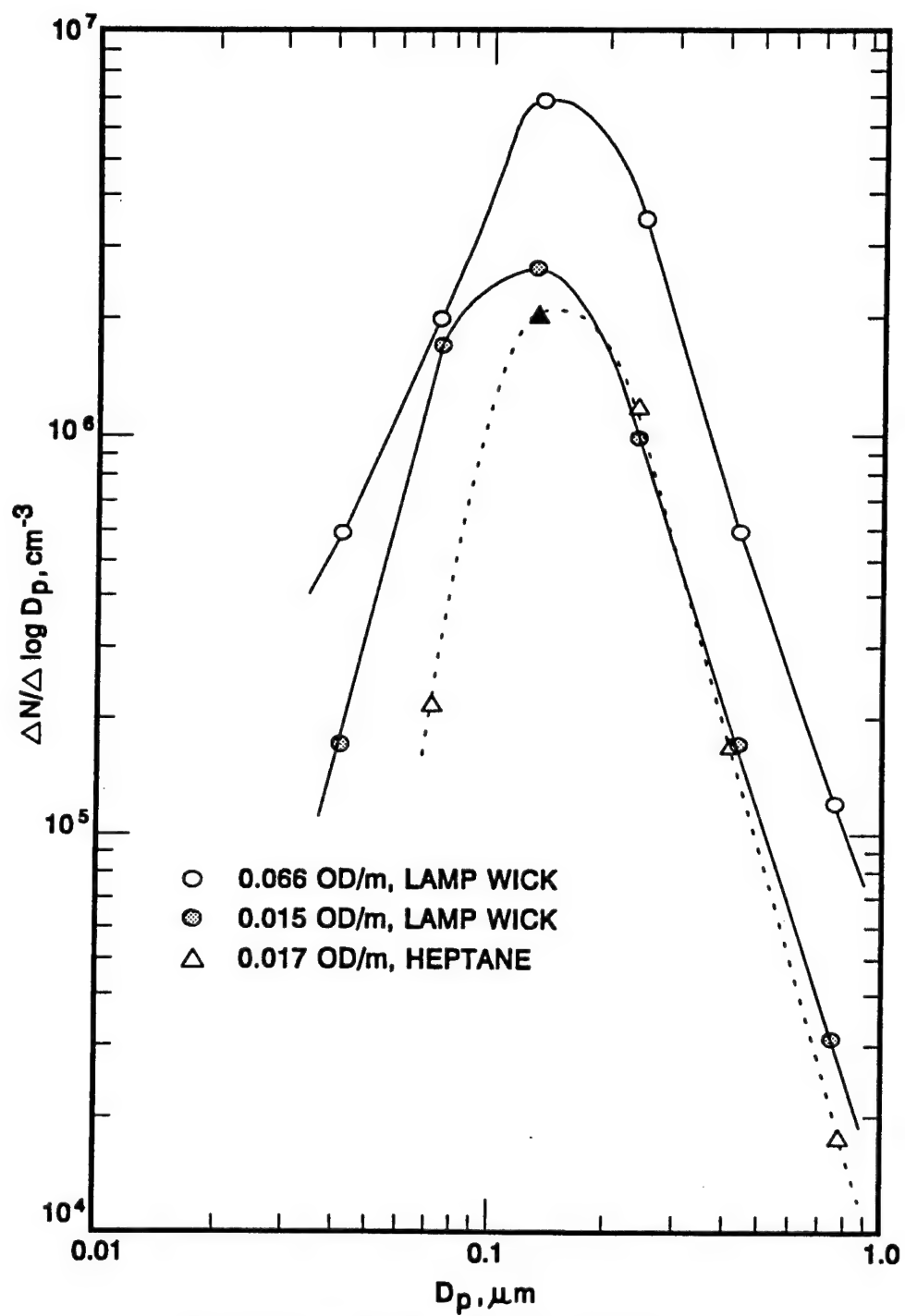
$$O = \left[1 - \left(\frac{T_s}{T_c} \right)^{\frac{1}{d}} \right] 100$$

where O = obscuration in percent per foot,
 T_s = detected optical power with smoke present,
 T_c = detected optical power with clear air
 d = distance of the air gap in feet.

This equation also applies in the metric system of units. Both the optical source and detector are broad band.

The particle size, shape, concentration, and composition of smoke is a function of the material being burned, smoldering versus flaming fires, age of the smoke, temperature of the smoke, and air movement.⁴ The particle size distribution of smoke from heptane and lamp wick sources, under standard conditions, peaks at an equivalent diameter slightly above 0.1 μm as shown in Figure 2. (N is the number of smoke particles per cubic centimeter and D_p is

Figure 2 - Particle Size Distribution for Lamp Wick and Heptane Smokes.



(Reprinted with permission from reference 4)

the particle size in micrometers.) A fast burning or flaming fire generates smaller smoke particles and greater particle concentrations, effectively shifting these curves to the left, with the peak equivalent diameters occurring well below $0.01\text{ }\mu\text{m}$. As smoke ages, the particles tend to coagulate into larger particles, shifting the distribution curves to the right and causing a lower particle concentration; this effect occurs over periods of minutes and hours. Cooler temperatures cause an increase in the size of the smoke particles; high fire temperatures shift the particle distribution curves to the left toward the smaller particles. Air movement tends to keep the smoke particles from coagulating together and therefore results in smaller size particles at greater concentrations.

STATE OF THE ART OF SMOKE DETECTORS

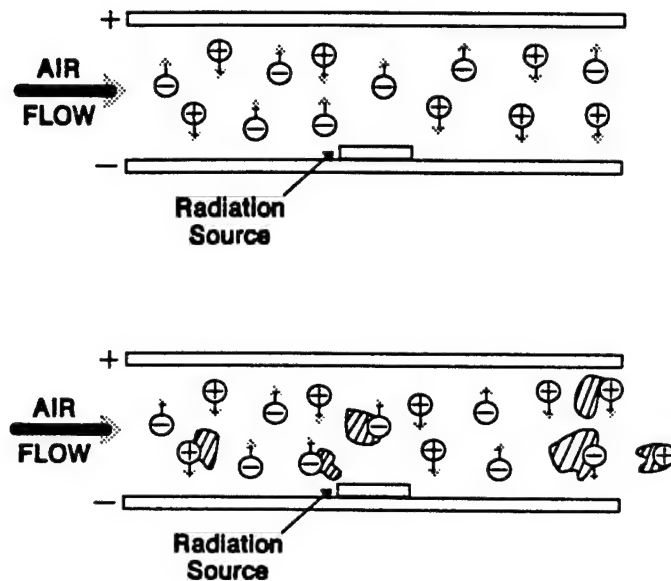
The principle kinds of smoke detectors in use today are the ionization chamber and the photoelectric types.⁵ Only the ionization type is generally applied onboard ship. The primary shortfall in performance is false alarms that are estimated to arise from water spray in the air, electromagnetic interference (EMI), and dirt coatings. There are a few newer types of smoke detectors under development, mostly based on optical technology, that may eventually become commonly used if they compare favorably in cost and overcome some of the problems associated with the ionization chamber and the photoelectric type smoke detectors.

IONIZATION SMOKE DETECTORS

The operating principle of the ionization chamber smoke detector is illustrated in Figure 3.⁴ As air molecules enter the test chamber, they are ionized by a low power radiation source. These ionized air molecules are drawn to charged collector plates and induce an electrical current in a circuit proportional to the number of charged particles (ions) per unit volume and the strength of the electric field. Under normal circumstances the velocity of the ions moving to the charged plates is relatively fast; the velocity of the ions flowing through the electric field determines the amount of ions being collected on the charged plates and establishes a baseline electrical current for clean air. When smoke enters the test chamber, the ionized air molecules attach to the smoke particles. The combined ionized air molecules and smoke particles are much larger than the air molecules alone and the velocity of movement toward the charged plates is significantly slowed. As a result, some of the ions escape from the test chamber by natural air convection currents and the received current decreases, indicating the presence of smoke. When the electrical current decreases below a preset value, an alarm is triggered.

Ionization smoke chambers can be designed to be bipolar and unipolar, referring to the presence of equalized numbers of ions in the chamber in the first case and unequal numbers of ions in the chamber in the second case. Both work on essentially the same principle. The unipolar chambers are somewhat more tolerant of high air flow rates.⁵

Figure 3 - Operating Principal of an Ionization Chamber Smoke Detector.



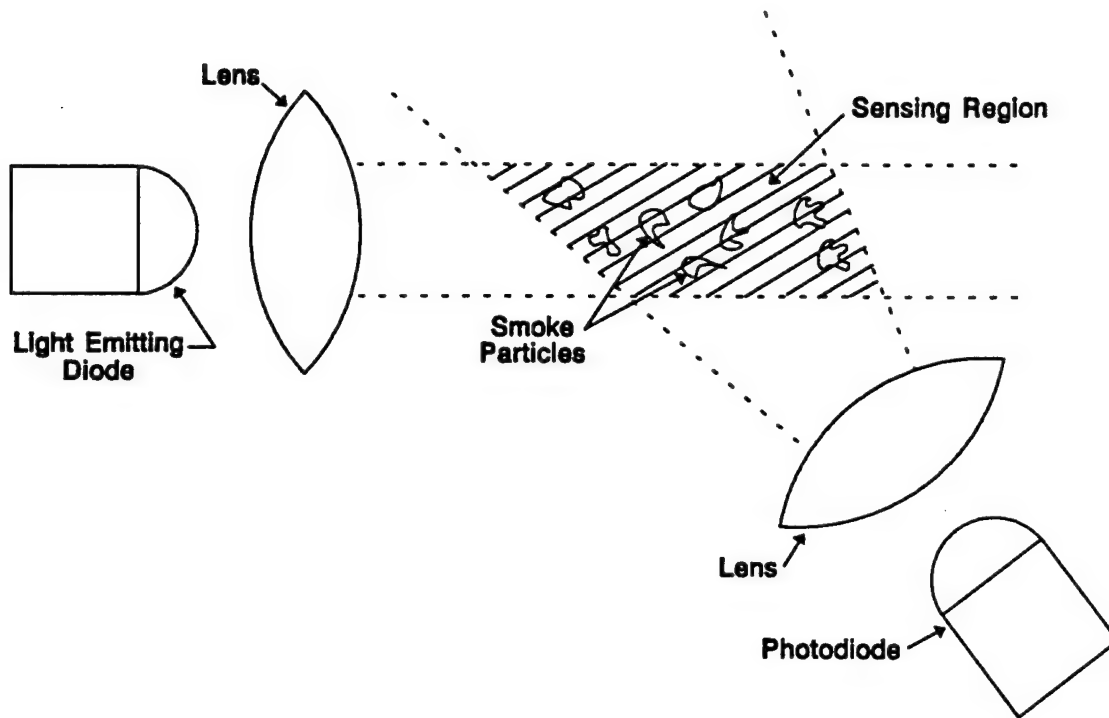
PHOTOELECTRIC SMOKE DETECTORS

Photoelectric smoke detectors utilize the scattering properties of smoke particles to measure smoke density as shown in the schematic in Figure 4. An optical source illuminates the test chamber in which the smoke enters by natural convection. A shield eliminates a direct light path from the source to the optical receiver so that no light is received when smoke is absent from the chamber. When smoke enters the test chamber, the smoke particles scatter light in all directions causing light to be collected on the optical detector; the received optical power is directly proportional to the smoke concentration present; it is also a function of transmitted power, particle size, shape, and composition, and receiver properties such as field of view, and detection efficiency.

SMOKE DETECTOR PERFORMANCE COMPARISON

Each smoke detector has its strengths and weaknesses. Figure 5 shows the relative sensitivity of ionization and photoelectric smoke detectors. In general, the ionization chamber is better at detecting very small particles such as those that would be generated in the very hot raging fires that are often caused by combat damage. Most of the peace time fires that must be detected onboard ship start as small smoldering fires that give off large particulate and might be better detected with the light scattering (or photoelectric) smoke detectors.

Figure 4 - Light Scattering Optics For a Photoelectric Smoke Detector.

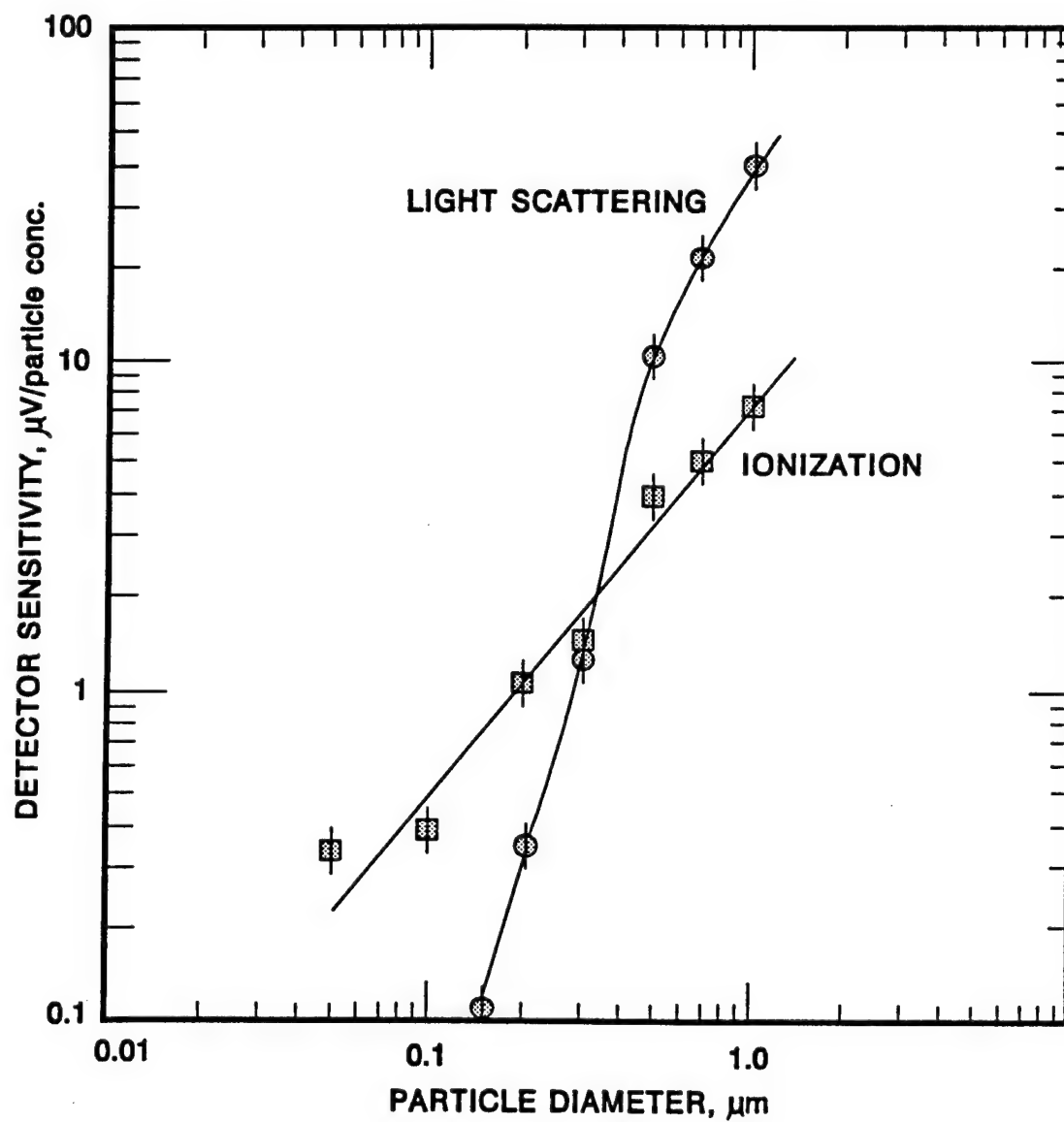


Advantages and disadvantages of ionization smoke detectors are the following: The primary advantage is low cost, partly arising from the high volume production as stimulated by the residential housing market. Ionization smoke detectors have high false alarm rates as every house owner knows that has mounted one next to a bathroom. Airborne water particles act like smoke particles, removing ions from the chamber and causing false alarms. Ionization smoke detectors do not distinguish between gray and black smoke.

Advantages and disadvantages of photoelectric smoke detectors are the following: The devices are simple to design and therefore low cost. They are subject to false alarms because visibility is measured not smoke density. Airborne dirt and droplets cause scattering the same way that smoke does leading to false alarms. Dirt and water droplets from condensation can collect on the optical surfaces, changing the sensitivity and therefore the detection threshold, again leading to false alarms. Only amplitude of the scattered optical signal is detected, meaning large particles are more likely to cause an alarm condition because they scatter light more strongly than the small particles. Photoelectric smoke detectors do not distinguish between gray and black smoke.

The US Navy uses smoke detectors designed to meet MIL-S-16032. The primary problem encountered onboard ship is false alarms, probably caused by airborne nonsmoke particles (or droplets) and electromagnetic interference. There is also no indication of smoke density since these are threshold sensors; thus the fire fighters presently have no visibility information when entering compartments.

Figure 5 - Detector Sensitivity for Ionization and Light Scattering Smoke Sensors.



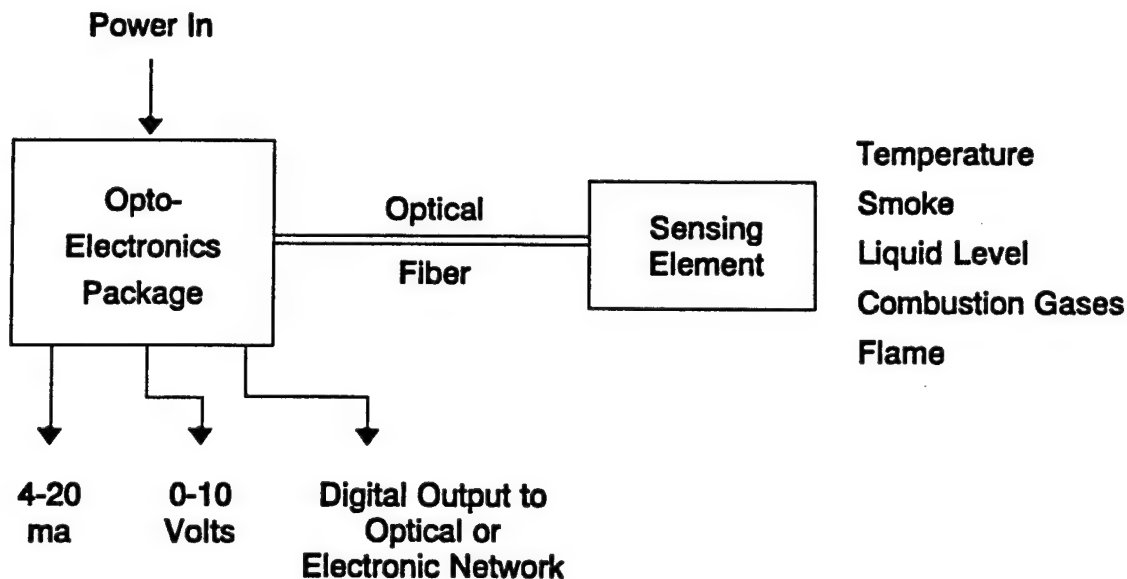
(Reprinted with permission from reference 4)

When designing new damage control systems that respond in essentially real time, every shipboard compartment must be monitored. Optical fiber technology offers new design implementations of the photoelectric smoke detectors as well as designs that offer continuous indications of the smoke density. The new smoke sensors should improve false alarm rates and enable more comprehensive smoke monitoring of ships without increasing maintenance burden for the ship's crew. Designs can take the form of an optical fiber data network using existing electrical smoke detectors or they can be completely new sensors that employ the inherent advantages of optical fiber technology while improving the operational performance.

OPTICAL FIBER SMOKE SENSOR DESIGN

Most optical fiber sensors have a schematic as shown in Figure 6, and consist of an electronics package, a sensor element, and a fiber cable.

Figure 6 - Optical Fiber Sensor, General Schematic for Damage Control Monitoring.



The opto-electronics package consists of four parts: power and support electronics, electro-optics, signal processing, and an output module. The power and support electronics module regulates and conditions the input power and provides power to on/off lights, cooling for laser diode sources, etc. The electro-optics unit converts electronic signals to, and from, the optical form. The signal processing unit converts the detected optical signals to a signal

proportional to the parameter being measured. The output unit converts the processed signal into one of the Navy standard data transmission formats.

The connecting fiber cable carries the optical signals to and from the sensor element. It is always fiber only and provides the electrical isolation necessary to eliminate electromagnetic interference effects.

The sensor element consists of either just optical fiber or miniaturized bulk optical components. The sensor element transduces the measurand (the parameter being measured) into an optical signal of variable amplitude, wavelength, phase, or polarization. The optical fiber sensors discussed in the following sections all utilize one of these four optical sensing techniques.

There are several methods of designing smoke sensors using optical fiber technology. Sensor types include power loss (obscuration), scattering, spectrometric, and fluorescent. All the optical fiber smoke sensor designs utilize the fiber to transmit light to and from a sensor element. Light is then launched through an air gap and interacts with smoke particles when they enter the air gap.

OBSCURATION OPTICAL FIBER SMOKE SENSORS

One way to detect the presence of smoke and to measure the smoke density is to simply transmit a beam of light across a gap and measure the optical power received as shown in Figure 7. As the smoke particles fill the air gap of the sensor, the received power decreases proportionally to the smoke density. The obscuration is a measure of the smoke density and is the normalized difference between the optical power transmitted into the air gap and the optical power received:

$$O = C \left[\frac{E_T - KE_R}{E_T} \right] 100 = C \left[1 - K \frac{E_R}{E_T} \right] 100$$

where O = obscuration (percent per foot)

E_T = optical power transmitted

E_R = optical power received

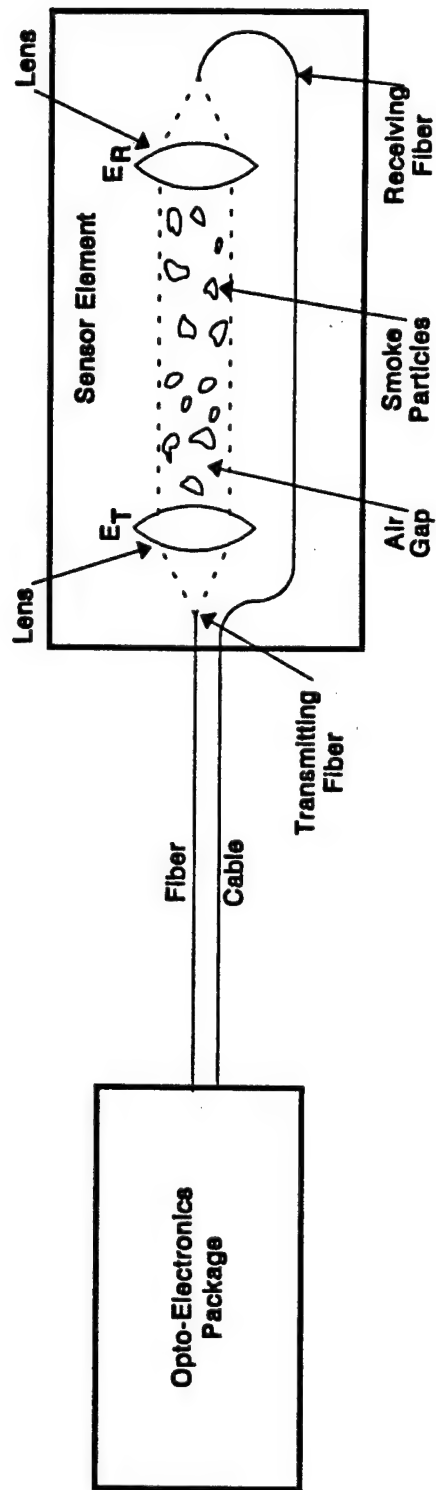
K = scaling constant required to make $E_s = E_T$ for clear air

C = an instrument constant

In its most basic form, this kind of obscuration smoke detector is sensitive to optical power changes, dirt coatings on the optical surfaces, and the presence of nonsmoke particles or droplets that absorb and scatter light. There are several methods of fixing these problems. For example, optical power transmitted can be detected with a monitor diode and used as a control signal to hold the transmitted light constant while dirt builds up on the optical surfaces.

The effect of dirt coatings can be eliminated by checking the time rate of change of the received optical power. Changes due to dirt accumulating on the optical surfaces occur over

Figure 7 - Obscuration Smoke Sensors Schematic.



$$\text{Obscuration} \approx C \left[\frac{E_T - K E_R}{E_T} \right] 100 = C \left[1 - K \frac{E_R}{E_T} \right] 100$$

time scales of days, weeks, months, and years, where as smoke causes changes in the received optical power in the time scale of seconds or minutes.

There is no adequate method of compensating for the presence of nonsmoke particles in the air gap that sometimes cause false alarms. Fortunately most smoke sensors are applied in areas where the atmosphere is much clearer than the 2% to 3% obscuration values of smoke that indicate the possible presence of a fire.

One other major disadvantage is that the air gap must be long, often being of the order of 1 meter. This is required because the received signal is compared to the power transmitted, meaning one is measuring the difference between two large numbers, causing noise and uncertainty on the smoke density indication.

SCATTERING OPTICAL FIBER SMOKE SENSORS

Adding a second optical receiver, offset a few degrees from directly forward (0 degrees) to measure the optical power scattered from smoke particles, results in an improved smoke sensor; the schematic of the scattering optical fiber smoke sensor is shown in Figure 8. (This sensor is an optical fiber implementation of the photoelectric smoke sensors with the addition of a forward scatter detected signal.) Use of the scattered optical signal along with the absorption optical signal provides two signals proportional to smoke density. The absorption optical signal decreases as a function of smoke density while the scattered optical signal increases as a function of smoke density.

The detection of the scattered energy is a critical function of the angle relative to forward scattering as shown by the analysis detailed in Appendix A. Forward scattering contains the most optical energy with the detected power decreasing as the angle changes from 0 degrees (forward) to 90 degrees. Forward scattering angles exceeding $\pm 10^\circ$ result in received optical signals that are too low for practical implementation of a smoke sensor. The design rule of thumb is to set the angle of the scattered light receiver as close to zero as possible without picking up light from the transit beam across the air gap.

For the configuration shown in Figure 8 and small quantities of smoke in the air gap, the operating equation of the scattering smoke sensor becomes:

$$O = C_2 \left[\frac{E_{RS}}{E_{RA}} \right] 100$$

where O = obscuration (percent per foot)

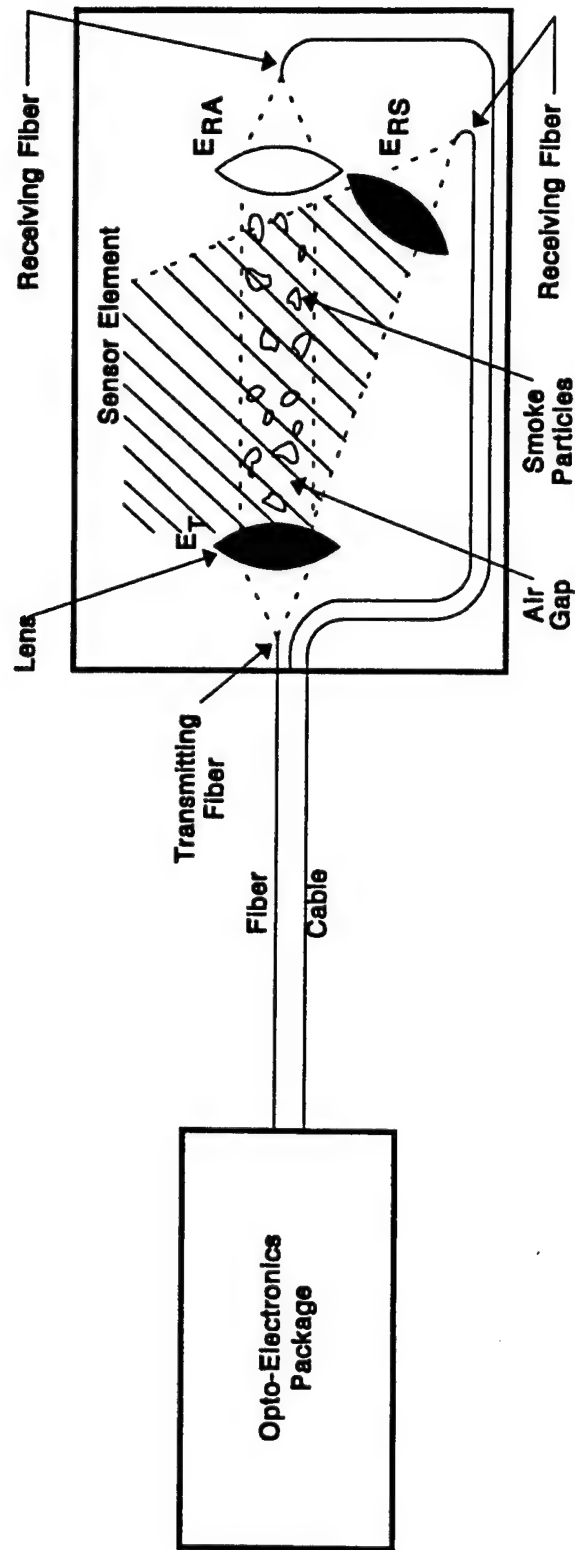
E_{RS} = received scattered optical signal

E_{RA} = absorption (forward scattered) optical signal

C_2 = an instrument constant.

Taking the ratio of the received optical powers removes the transmitted optical power from the equation and compensates for the accumulation of dirt and soot coatings on the optical surfaces. It also keeps the signal processing very simple.

Figure 8 - Scattering Fiber Optic Smoke Sensor Schematic.



$$\text{Smoke Density} = \frac{\text{Scattered Light}}{\text{Transmitted} - (\text{Absorbed and Scattered}) \text{ Light}} \approx C_2 \frac{E_{RS}}{E_{RA}}$$

Another configuration of the scattering optical fiber smoke sensor is shown in Figure 9. This configuration maximizes the signal to noise ratio by collecting nearly all of the scattered light rather than just a small portion as is true for the photoelectric smoke detector shown in Figure 4 and the scattering optical fiber smoke sensor shown in Figure 8. Lens L_1 collimates the transmitted optical power from the incoming fiber. Lens L_2 collects and columnates the scattered optical power. Lens L_4 and L_5 focus the scattered optical energy onto the end of the scattering receiving fiber. Lens L_3 focuses the forward transmitted optical power onto the optical absorption receiving fiber. The diameters of lens L_2 and L_4 are set to collect all the optical power out to ± 10 degrees. The diameter of lens L_3 is set as sufficiently small to avoid interrupting the scattered light collected by lens L_2 , and sufficiently large to collect all the forward transmitted optical power.

One major advantage of the scattering optical fiber smoke sensor is that compensation for dirt and water coatings of the optical surfaces is inherent because the processing is a ratio where the first order effect of the dirt coatings drops out of the transfer function. Rate of change of the smoke obscuration signal can also be used to provide additional compensation for dirt coating of the optical surfaces. Slow drifts over a matter of days can be ignored as smoke particulate arrive in the sampling chamber in a time frame of seconds or minutes.

Another major advantage of the scattering smoke sensor is that shorter path lengths are possible than for optical power absorption smoke sensors because the scattered optical signal starts at zero when the air is clean. The signal processing does not utilize the difference between two large signals.

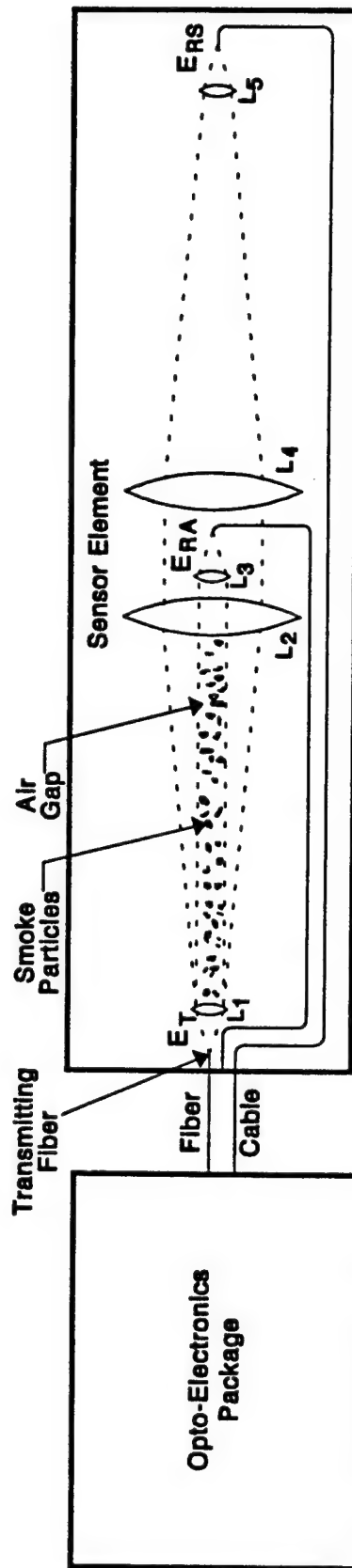
The principle disadvantage of the scattering smoke sensor is that nonsmoke particles will be detected as smoke particles.

A model of the scattering smoke sensor was constructed in the laboratory and checked for operation with smokes generated by cigarettes, cotton wicks, and diesel fuel. The wavelength of the sources used were 633, 830, and 1300 nanometers. Shorter wavelengths cause higher scattering signals from the smoke particles because the wavelength of the light is closer to the diameter of the particles. Examination of the smoke particle size distribution for all expected cases of composition, temperature, age, air movement, and smoldering versus flaming fires, ⁴ shows that the best choice of wavelengths is in the area 200 to 400 nanometers. All kinds of smoke contain particles with diameters in this size range. No experiments at these wavelengths were done because we had no such sources in our laboratory; this should be part of a follow-on 6.3 development program.

SPECTROMETRIC OPTICAL FIBER SMOKE SENSORS

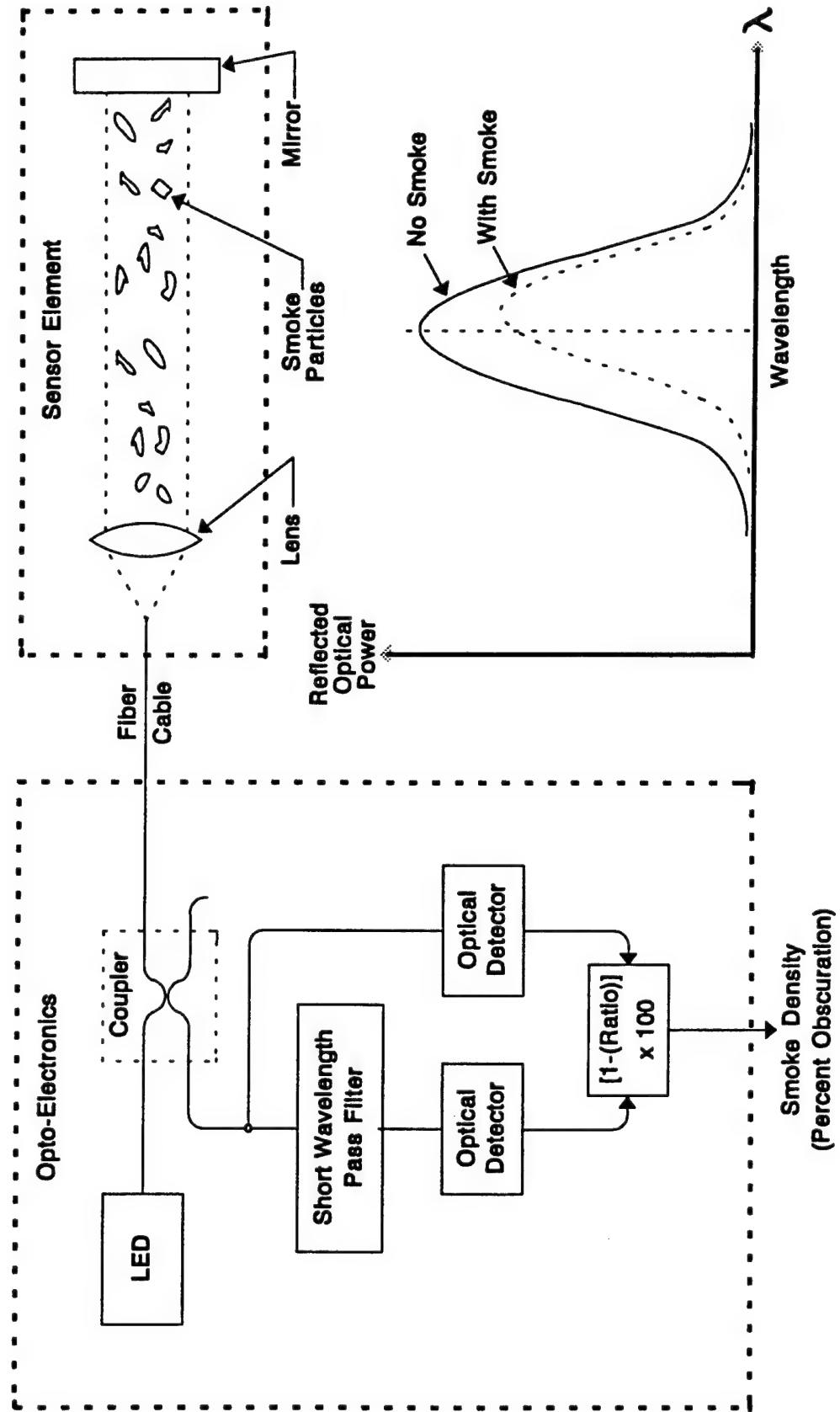
Optical power absorption smoke sensors can be designed to utilize the size distribution of the smoke particles in the air gap as an indicator of the smoke obscuration. When smoke particles enter the sample chamber, the spectral distribution of the received optical power changes because of wavelength selective absorption and scattering. The schematic for the spectrometric smoke sensor is shown in Figure 10. The light from an optical source - an LED was used in our experiments - illuminates an air gap between a lens and a mirror. The same fiber is used in both transmitting and receiving modes. The opto-electronics circuitry

Figure 9 - Scattering Optical Fiber Smoke Sensor Schematic Using Large Collecting Lens.



$$\text{Smoke Density} = \frac{\text{Scattered Light}}{\text{Transmitted - (Absorbed and Scattered) Light}} \approx C_2 \frac{E_{RS}}{E_R}$$

Figure 9 - Schematic Diagram for a Spectrometric Fiber Optic Smoke Sensor.



measures the shift in reflectance spectrum due to the presence of smoke particles and correlates that shift with the smoke density and obscuration.

The shift in the reflected optical power absorption spectrum is detected by calculating the ratio of the optical power in the short portion of the spectrum relative to the long portion of the spectrum. The reflected optical power from the air gap is coupled into the optical detection diodes via the coupler at the output of the LED. An optical filter is inserted that passes only the short wavelengths of the LED spectrum. Cutoff wavelength of the short wavelength pass filter is picked to exactly split the optical power evenly between the long and short wavelengths of the transmitted LED spectrum. The remainder of the processing circuitry forms the ratio of the short to long wavelength optical power and subtracts that ratio from one so that the output for clean air is zero. When smoke enters the chamber, the shorter wavelengths are absorbed more than the long wavelengths because of two factors. There are many more particles present with smaller diameters and the dimensions of these smaller smoke particles are closer to resonance with the short optical wavelengths of the LED spectrum. (Resonance causes much greater power absorption.) This biases the reflectance spectrum toward longer wavelengths decreasing the ratio of short wavelength power to long wavelength power, O_s over O_L , and increasing the output calculated obscuration. The output of the spectrometric smoke sensor is given by:

$$O = \left[1 - \frac{O_s}{O_L} \right] 100$$

where O = obscuration (percent per foot)

O_s = optical power absorbed in the short wavelength region

O_L = optical power absorbed in the long wavelength region.

More details of the scattering properties of light by smoke particles can be found in Appendix A of this report.

An experimental model of the spectrometric smoke sensor was built and tested on the ex-USS SHADWELL as documented in Appendix B. Air gap in the sensor was 2 inches giving a round trip optical path length of 4 inches, generally much shorter than most optical smoke sensors. The wavelength of the LED source was 850 nanometers. The fiber used was 100/140 micrometers.

The wavelength of the optical source should be picked to more closely match the equivalent-diameter of the smoke particles.^b This would cause much greater absorption of the optical energy by the smoke particles because they would be closer to resonance. The result would be an increase in the sensitivity of the smoke sensor and a decrease in the effect of noise in the optical circuit. Tolerance to dirt and water coating on the optical surfaces would be increased with the increased signal to noise ratio. Examination of the particle size distribution of the smoke particles from reference 4 shows that setting the optical source wavelength in the range of 200 to 400 nanometers would encompass all the possible sizes of

b) Smoke particles are not always spherical. The term "equivalent-diameter" is here used to denote the dimensions of the resulting sphere if the irregular shaped smoke particles were reshaped into a sphere.

smoke particles. The operating wavelength would be just above (slightly longer than) the peak of the size distribution retaining the bias effect on the reflectance spectrum.

Another method of increasing the sensitivity and reducing noise effects would be to use two optical sources. Separating the source wavelengths by tens or hundreds of nanometers would increase the bias effect and therefor increase the sensitivity of the measured signals to the presence of smoke .

A major advantage of the spectrometric smoke sensor is reduced sensitivity to the presence of ambient light. Since the power in the reflected optical spectrum is split between long and short wavelengths, and a ratio formed between the two, the portion of ambient light detected is also split giving a first order compensation. The degree of compensation is dependent on the balance of optical power between the power in the long and short wavelengths of the reflectance spectrum. More study and measurements are required to determine the optimum split of the ambient light spectrum for most shipboard conditions.

Another advantage of the spectrometric smoke sensor is improved tolerance to water coatings on the optical surfaces. As long as the water coatings affect the long and short wavelengths equally, the detected ratio, O_s/O_L , remains the same and there is no effect on the calculated smoke obscuration in the instrument.

There is also an advantage to using the spectrometric smoke sensor onboard ship in the area of standardization of opto-electronic packages. The most likely optical fiber sensors to be applied in damage control monitoring systems to measure temperature, liquid level, and pressure are the Fabry-Perot types; the opto-electronics packages used for the spectrometric smoke sensor and Fabry-Perot sensors are identical. This means that the same opto-electronics package can be used for all the damage control sensors (except flame) presently used onboard ship. Unit measurement cost is expected to drop because the opto-electronics packages are the most expensive part of optical fiber sensors and could be purchased in much greater volume by the Navy.

The spectrometric optical fiber smoke sensor shares the same false alarm problem due to the presence of other airborne particulate. All types of smoke sensors and detectors, including the ionization, photoelectric, optical power absorption, scattering, and spectrometric sensors, interpret the presence of dust and dirt particles as smoke. This problem is reduced by the fact that in most compartments the natural cleanliness of the air is much below the 2 to 3 percent obscuration values that are commonly used to detect starting of fires.

FLUORESCENCE OPTICAL FIBER SMOKE SENSORS

Do smoke particles have fluorescent properties? And could that fluorescence be used as a design basis for a smoke detector that would not only detect critical levels of smoke but would also determine what materials were burning since each material would fluoresce at a different wavelength? Knowing what material is burning is very important information for determining fire fighting strategy. Even though the design of a fluorescent smoke detector is highly speculative at this time, an investigative program is suggested to determine if smoke has fluorescent properties and if they could be used to design a smoke detector.

COMMERCIALLY AVAILABLE OPTICAL FIBER SMOKE DETECTORS^c

Smoke detectors and sensors based on optical fiber technology are available in several types at the time of this writing. These authors have not done a comprehensive survey of company products at this time but have gained significant information from our contacts in the private sector. There is at least one model of optical power absorption sensor available that generates a continuously varying signal proportional to smoke obscuration over the range of 2 to 9 percent; there is another that gives an alarm when the smoke obscuration enters the range of 2 to 7 percent obscuration. There is an experimental model available of the optical fiber scattering smoke sensor. The optical fiber spectrometric smoke detector utilizes a commercially available opto-electronics package; the sensor design could easily be transferred to private industry and marketed within a short time. (The opto-electronics package for the optical fiber spectrometric smoke detector can also be used to measure temperature, liquid level, and pressure.)

SUMMARY

Optical fiber smoke sensors are ready for transition to a 6.3 advanced development program. They have been demonstrated to function properly both in a laboratory smoke chamber and on the ex-USS SHADWELL. New designs based on scattering and wavelength shift of the absorption spectrum offer performance improvements in the areas of greater information availability (continuous measurement as opposed to threshold detection), and reduced false alarms due to dirt and water coatings on the sensing surfaces.

Optical fiber smoke sensors, at the present stage of development, have a difficult time competing in the area of cost with commercially available smoke detectors from private industry that are used in residential and industrial applications. There are several reasons for being optimistic about reducing cost. Monitoring every compartment onboard ship, as is now being seriously discussed within the Navy, will greatly increase the volume of sensors purchased and therefor reduce unit measurement cost. Using multiplexing schemes presently under development at CDNSWC and NRL will also reduce unit measurement cost. Other methods of reducing cost are standardizing on one type of sensor as suggested above, and utilizing integrated optics. It is reasonable to expect that the cost of optical fiber smoke sensors will drop drastically if application volume rises to just a small fraction of the present smoke detector market.

One motivation for using fiber sensors is the availability of continuously variable indications wherein smoke density data are fed to the information management systems for damage control. This would improve the information required to determine fire fighting strategy. Another motivation for using optical fiber smoke sensors is the ability to construct a

c) No company names will be used herein to avoid the appearance of endorsing any given product. Readers are encouraged to contact the authors directly for the names of companies that produce commercially available optical fiber smoke detectors.

shipwide network of smoke sensors using well known fiber data network technology. When fiber smoke sensors are used there is absolutely no problem with electromagnetic interference. Optical fiber smoke sensors, if fully developed offer reduced false alarms when compared with conventional electrical smoke detectors.

REFERENCES

1. Whitesel, Henry K., Donald L. Fairhead, and John K. Overby, Shipboard Fire Detection with Optical Fiber Temperature Measurement, Carderock Division Naval Surface Warfare Center Technical Report CARDEROCKDIV-MRD-80-93/17, April 1993.
2. Whitesel, Henry K., and Patricia Tatem, "Detection of Shipboard Fires with Fiber Optic Temperature Sensors, Applications of Fiber Optic-Based Sensors in Industry and Vehicles, SPIE Vol 2072A, 8-9 Sept 1993.
3. Smoke Detectors for Fire Protective Signaling Systems, Underwriters Laboratories Standard UL268, American National Standard ANSI/UL268-1988, Third Edition, May 1989.
4. Lee, G. k., and George Mulholland, Physical Properties of Smokes Pertinent to Smoke Detector Technology, National Bureau of Standards Report NBSIR 77-1312, Nov 1977.
5. Bukowski, Richard W., and George W. Mulholland, Smoke Detector Design and Smoke Properties, National Bureau of Standards Technical Note 973, Nov 1978.

APPENDIX A

ANALYSIS OF LIGHT SCATTERING BY SMOKE FOR FIBEROPTIC SMOKE DETECTOR DESIGN

An analysis of the phenomena of the scattering and absorption of light by smoke particles was undertaken in order to develop a model that can be used for the design of a fiberoptic-based instrument that can detect smoke in a shipboard compartment. The model developed here uses experimentally measured values for smoke generated by combustion of heptane to derive scattering predictions as a function of fiber parameters.

The passage of electromagnetic radiation through a medium is generally accompanied by the removal of a fraction of the energy from the incident beam. This fraction may be partly absorbed within the medium, and may be partly scattered. The characteristics of the scattered radiation are determined by the wavelength of the incident radiation, the complex refractive index ($m = n_1 - in_2$) of the medium, and the size as well as the shape of the discrete particles of the medium. These are the main issues which will be addressed to develop an optical-fiber based smoke detector for use on-board ships.

Smoke detection technology is primarily concerned with the aerosol component of smoke, even though smoke generated from fire-related sources consists of both gases and aerosols. The smoke aerosol can have a wide range of properties depending on the material burned and the condition in which it burns (smoldering or flaming). Some of the properties are the following:

- liquid drops or solid particles (possibly including an adsorbed liquid phase),
- shape can vary from spherical to chain agglomerates, and
- optical properties vary from very absorbing for the black sooty smoke to almost transparent for some smokes from smoldering fires.

From a detection point of view, the most significant property is its size distribution, which is discussed later.

The numerical evaluation of the parameters of the radiation scattered by a particle very small compared to the wavelength is very simple and straight forward and was first derived by Rayleigh [5,6]. The expressions for the radiation scattered by a sphere

whose radius (a) is comparable to, or greater than, the wavelength were first derived by Mie [5,6]. The expressions for Mie scattering involve series whose terms contain Bessel functions of half-integral order (spherical Bessel functions) with complex argument, and first and second derivatives of the Legendre polynomials. Furthermore, the number of terms required for evaluating the series is of the order of the size parameter x ($x=2\pi a/\lambda$). Hence, the computations of reliable Mie scattering for large spheres can be described as difficult, tedious and time consuming.

The light signal scattered from a particle is affected by particle diameter, complex refractive index, scattering angle, scattering volume, light wavelength, and particle shape. The effect of particle size falls into three regions defined essentially by the ratio of the particle size to light wavelength.

These three regions are given below:

| | |
|-----------------|------------------------------|
| Rayleigh Region | $d < 0.1 \lambda$ |
| Mie Region | $0.1\lambda < d < 4 \lambda$ |
| Bricard Region | $d > 4 \lambda$ |

In the Rayleigh scattering region, the output signal is essentially proportional to the sixth power of the particle diameter. The upper limit of the Mie region is not clearly defined as it varies as a function of particle refractive index. At the Mie-Rayleigh boundary, the output signal is proportional to the particle diameter to the sixth power and can oscillate in a damped sinusoidal manner until at the Mie-Bricard boundary it is proportional to the square of the particle diameter. The frequency of oscillation is a function of the refractive index of the particle. For particles larger than about 4λ , the theories of geometric optics (Bricard, Fraunhofer diffraction) predominate. In this region the signal is proportional to the particle diameter squared.

EXPRESSIONS FOR MIE SCATTERING

In order to describe the scattering process fully, it is necessary to represent a beam of radiation as a vector or as a one-column matrix (I) with four elements. In the Stokes

representation [8], the first two elements of this matrix, noted by I_e and I_r , represent the specific intensities of the beam in two directions e and r , respectively. The directions e and r are mutually perpendicular to each other, and the e - r plane is perpendicular to the direction of propagation of the radiation under study. The other two elements, viz., I_u and I_v , are needed for defining the direction of polarization with respect to the e - r plane, and the ellipticity of the beam, respectively. Further details about the Stokes parameters and their relationships to the conventional radiation parameters can be found in several places [5].

The expressions for the radial scattering by a sphere of radius a , and of material with a complex index of refraction, have been derived by Van de Hulst [5], and also by Born and Wolf. We shall therefore enumerate the final results only. Let I_i and I_s respectively represent the Stokes parameters of the radiation incident on, and scattered by, a sphere with e component parallel to the plane of scattering. Then

$$I_s = F' I_i \quad (1)$$

where F' is a four-by-four matrix referred to as a "transformation matrix" by Van de Hulst. It has the following form:

$$F' = \begin{vmatrix} M_2 & 0 & 0 & 0 \\ 0 & M_1 & 0 & 0 \\ 0 & 0 & S_{21} & -D_{21} \\ 0 & 0 & D_{21} & S_{21} \end{vmatrix} \quad (2)$$

The matrix F' and hence the matrix I_s are functions of the parameters

$x = 2\pi a/\lambda$, where λ is the wavelength of the incident radiation,

$m = n_1 - n_2$, index of refraction of the material of the sphere with respect to its surrounding, and

q = the angle between the direction of the incident and that of the scattered

radiation.

Van de Hulst also noted that only three elements of F' are independent, the interrelationships being

$$(3) \quad S_{21}^2 + D_{21}^2 = M_2 M_1.$$

In order to evaluate these elements, one first defines the complex amplitudes $S_1(x, m, q)$ and $S_2(x, m, q)$ for the scattered radiation as

$$S_1(x, m, \theta) = \sum_{n=1}^{\infty} \frac{(2n+1)}{n(n+1)} [a_n(x, m) \Pi_n(\mu) + b_n(x, m) \tau_n(\mu)] \quad (4a)$$

and

$$S_2(x, m, \theta) = \sum_{n=1}^{\infty} \frac{(2n+1)}{n(n+1)} [b_n(x, m) \Pi_n(\mu) + a_n(x, m) \tau_n(\mu)], \quad (4b)$$

where $\mu = \cos q$. Then,

$$M_1 = S_1 S_1^*, \quad (5)$$

$$M_2 = S_2 S_2^*, \quad (6)$$

$$S_{21} = \frac{1}{2} (S_2 S_1^* + S_1 S_2^*), \text{ and} \quad (7)$$

$$D_{21} = \frac{i}{2} (S_2 S_1^* - S_1 S_2^*). \quad (8)$$

The functions $a_n(x, m)$ and $b_n(x, m)$ are given by

$$a_n(x,m) = \frac{\psi'_n(mx)\psi_n(x) - m\psi_n(mx)\psi'_n(x)}{\psi'_n(mx)\xi_n(x) - m\psi_n(mx)\xi'_n(x)} \quad (9)$$

and

$$b_n(x,m) = \frac{m\psi'_n(mx)\psi_n(x) - \psi_n(mx)\psi'_n(x)}{m\psi'_n(mx)\xi_n(x) - \psi_n(mx)\xi'_n(x)} \quad (10)$$

$\psi'_n(z)$ and $\xi'_n(x)$ are the derivatives of $\psi_n(z)$ and $\xi_n(x)$ with respect to z and x , respectively, where

$$\psi_n(z) = zJ_n(z), \quad (11)$$

$$\xi_n(x) = x[J_n(x) - iY_n(x)], \quad (12)$$

$$\psi'_n = zJ_{n-1}(z) - nJ_n(z), \quad (13)$$

and

$$\xi'_n = x[J_{n-1}(x) - iY_{n-1}(x)] - n[J_n(x) - iY_n(x)]. \quad (14)$$

The functions J_n and Y_n are the spherical Bessel functions of the first and second kind, respectively. The following recurrence relationships and initial values for setting up the recurrence procedure can be found in any of the standard mathematical books:

$$f_{n+1}(z) = \frac{2n+1}{z} f_n(z) - f_{n-1}(z), \text{ where } f_n(z) \text{ is } J_n(z) \text{ or } Y_n(z), \quad (15)$$

$$J_{-1}(z) = -Y_0(z) = \frac{\cos z}{z}, \quad (16)$$

and

$$J_0(z) = Y_{-1}(z) = \frac{\sin z}{z}. \quad (17)$$

The phase functions $\pi_n(\mu)$ and $t_n(\mu)$ can be expressed in terms of the Legendre polynomials as

$$\pi_n(\mu) = \frac{dP_n(\mu)}{d\mu} \quad (18)$$

and

$$\tau_n(\mu) = \mu\pi_n(\mu) - (1 - \mu^2) \frac{d\pi_n(\mu)}{d\mu}. \quad (19)$$

Besides the elements of the transformation matrix F' , other terms of considerable importance are the dimensionless constants referred to as "efficiency factors" by Van de Hulst. Q_e , the efficiency factor for extinction, which is the ratio of the total amount of energy removed from the incident beam to the geometric cross section of the particle, can be obtained from the values of a_n and b_n only by

$$Q_e(x, m) = \frac{2}{x^2} \sum_{n=1}^{\infty} (2n+1) [\operatorname{Re}(a_n) + \operatorname{Re}(b_n)]. \quad (20)$$

The symbol Re stands for the real part of the quantity in parenthesis. Q_s , the efficiency factor for scattering, is given by the following expression:

$$Q_s(x, m) = \frac{2}{x^2} \sum_{n=1}^{\infty} (2n+1) [|a_n|^2 + |b_n|^2]. \quad (21)$$

If there is no absorption, i.e., $n_2 = 0$, then $Q_e = Q_s$. Otherwise, Q_a , the efficiency factor for absorption, is given by

$$Q_a = Q_e - Q_s. \quad (22)$$

Another dimensionless quantity of considerable interest is the so-called "asymmetry factor" represented by $\overline{\cos \theta}$, and given by

$$\overline{\cos \theta} = \frac{4}{x^2 Q_s} \sum_{n=1}^{\infty} \left(\frac{n(n+2)}{n+1} \operatorname{Re}(a_n a_{n+1}^* + b_n b_{n+1}^*) + \frac{2n+1}{n(n+1)} \operatorname{Re}(a_n b_n^*) \right). \quad (23)$$

The value of Q_p , efficiency factor for radiation pressure, can be obtained using the following

$$Q_p = Q_e - \overline{\cos \theta} Q_s. \quad (24)$$

OPTICAL FIBER SMOKE SENSOR DEVELOPMENT

BASIC DETECTOR MODEL

The basic smoke detector design to be considered is as shown in Figure 1. Here light emanating from the end of input fiber creates a cone of light within the housing of the detector, and this light is scattered and transmitted by the smoke within the housing. If the density of particles within the smoke is low, a relatively large percentage of this exiting light is received by the parallel receiving "reference" fiber that has its end positioned directly across the housing. In this case, the light scattered outside of the normal cone defined by the numerical aperture of the fiber will be small. If instead the density of the smoke is high, a smaller portion of the light is received by the opposite parallel fiber. The scattering equations developed may be used to determine the scattering-induced loss caused by the smoke as well as the off-axis particle scattering and reception of the off-axis receiving fiber.

To illustrate the basic principle, let us assume that the optical power in the input, multimode fiber with an numerical aperture of 0.2 is 1 mW. Also, assume that the diameter of the smoke detector housing is 10 cm. Then, if the off-axis fiber is positioned at an angle of, for example, 45° with respect to the input fiber, the power received with no smoke present is approximately 0.006 nW from simple geometry, assuming that the NA of the receiving fiber is also 0.2 [3]. The power received by the on-axis fiber is similarly calculated to be approximately 0.045 mW. This suggests that the proposed combination of on-axis and off-axis receiving fibers may be able to discriminate between the conditions of smoke and no-smoke. Thus we need to consider the optimal positioning of the off-axis fiber or the specification of the numerical aperture of the fiber to increase sensitivity.

We have reviewed Mie scattering theory, and we will now show how the particle size distribution characteristics of smoke varies, and how it could be used to determine the angular scattering profile of the smoke within the housing volume of a smoke detector. This effect of such profiles, which were assumed to vary as functions of 1) the type of material causing the fire producing the smoke, and 2) the time of duration of the fire after its beginning, could then be determined for different geometries of smoke detector.

We received detailed information concerning the physical properties of smoke [1] and

the design of several optical smoke detectors which use bulk optical components rather than optical fibers for light generation and detection [2]. From this graphical, experimental data and information we have been able to back-calculate the parameters needed to assemble a mathematical Mie scattering model

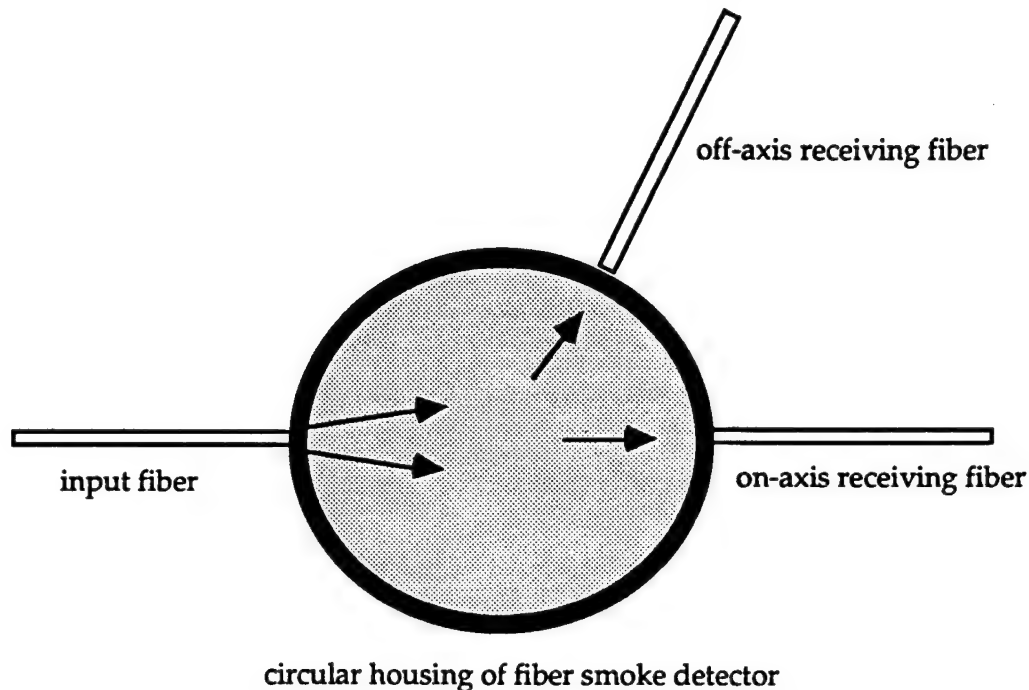


Figure A1- Geometry of Circular Housing of Fiber-Based Smoke Detector

describing the effect of the smoke on the performance of the optical fiber-based smoke detector design. Because the information is available in graphical form rather than a closed form equation, analysis requires a point-by-point construction of the scattering parameters.

Data required to perform the numerical calculations to determine the received light has been obtained from references [1, 2]. Specifically, Figure 8 in [1] shows the particle size distribution in particular types of lamp wick and heptane flames. We will assume that this type of smoke is typical of smoke generated by some types of fires on board ships. Because this data is not available in an analytical form, the numerical calculation based upon Figure 8 in [1] would require a full digitization of the curve of $DN/D\log D_p$. However, a uniform size distribution has been derived in [1], and plotted in terms of reduced variables y and h . The number distribution is reduced by the total number of particles in the size distribution, $N(t)$, and the diameter has been reduced by

a quantity related to the average diameter for the size distribution, $(V/N)^{1/3}$ for that particular smoke. Thus

$$y = DN/D \log D N(t) , \text{ and} \quad (25)$$

$$h = D(N(t)/V)^{1/3}. \quad (26)$$

This data includes fresh smoke as well as aged smoke, smoke generated in both the flaming and smoldering modes, whitish smoke and black sooty heptane smoke, and smoke generated under different air flow conditions. The numerical variation in the size distribution has been greatly reduced by using the reduced variables.

The reduced versions of the algebraic size distribution [1] and a log-normal size distribution [1] are given by the equations

$$y = 1.38h^3(h^3+0.2)^{-2} \quad \text{Junge-like} \quad (27)$$

and

$$y = 1.73 \exp[-(\ln 1.23h/0.744)^2] \quad \text{Log-normal with } s=1.7 \quad (28)$$

On plotting the above equations, it appears that both the algebraic and log-normal distribution fit the data (figure 2) [1]. It has been shown that the reduced algebraic distribution is only weakly affected by aging due to coagulation, as is also the case experimentally [1]. This means that the algebraic distribution could be used as a model size distribution not only for a variety of smokes, but also for smokes at various stages of aging. It has been observed that the log-normal distribution fits closely with the data for heptane. Thus the results of this model will be used in the development of the model for the smoke detector.

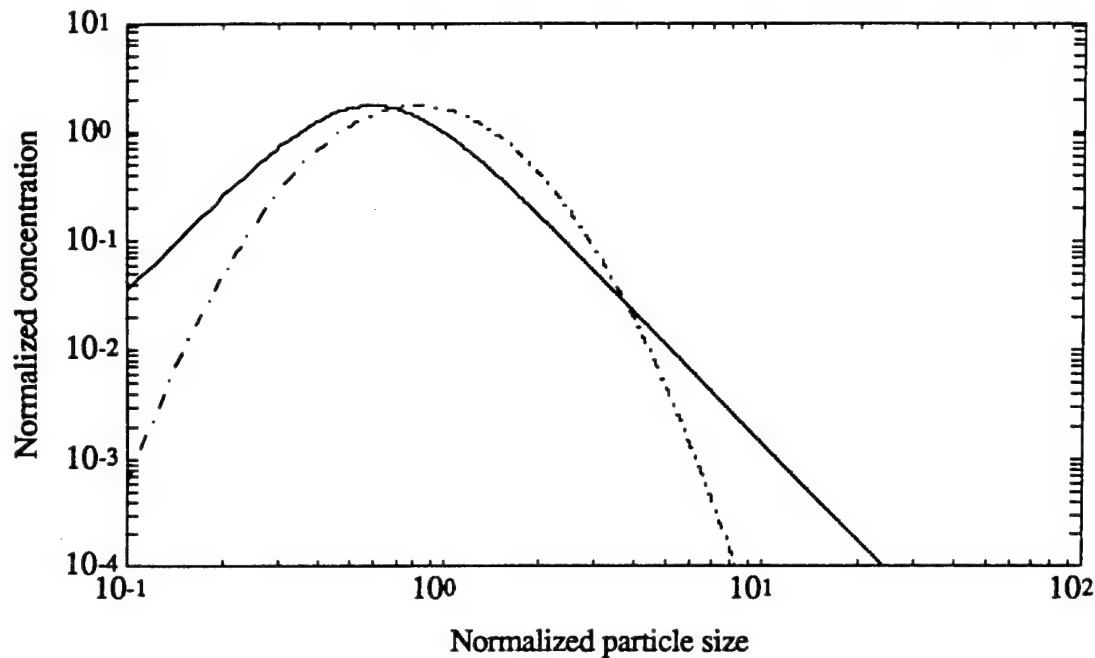


Figure A2- Algebraic (solid line) and Log-normal (dotted line) Distributions

MODELING OF MIE SCATTERING FROM SMOKE PARTICLES IN DETECTOR HOUSING

In the simple model we have adopted, we begin by assuming that the input light from the input fiber is a plane wave that travels through the scattering region and is scattered and attenuated by the smoke in the region. This model may be improved by considering the numerical aperture of the fiber, and the nonplanar nature of the input field, once data concerning smoke particle size establishes the operation of the sensor.

We also assume that within the volume of the sensor housing, there are N particles per unit volume at some time t . This number of particles can change with time, according to the way that the smoke develops. We consider the smoke particles to be spherical dielectric scatters of identical radii a within vacuum.

The intensity scattered per unit volume in a given direction is then N times the intensities calculated for one particle from a solution to the vector wave equation. Specifically, the scattered light intensity is

$$I = N \frac{I_0(i_1 + i_2)}{2k^2 r^2} \quad (29)$$

in which the terms i_1 and i_2 refer, respectively, to the intensity of light vibrating perpendicularly and parallel to the plane through the directions of propagation of the incident and scattered beams, and k is the propagation vector. By vibration, we mean vibration of the electric vector. Tables typically give i_1 and i_2 in terms of angle and distance, so the intensity of the light received at output fibers at any position can be determined directly. The degree of polarization is then

$$\frac{i_1 - i_2}{i_1 + i_2} \quad (30)$$

The intensity I of the proceeding beam above decreases in a distance l between the input fiber and the output fiber by the fraction e^{-gl} , where the extinction coefficient g is computed from

$$\gamma = N\pi a^2 Q_{\text{ext}} \quad (31)$$

independently of the state of polarization of the incident light. At the same time the proceeding wave is retarded. Here, Q_{ext} and $S(0)$ used below are efficiency factors which are tabulated for scattering particles of different geometries. Weakening and retardation are described together as the effect of a complex refractive index of the medium, i.e. as

$$\tilde{m} = 1 - iS(0)2\pi Nk^{-3}, \quad (32)$$

where the medium refers to the air containing the scattering particles. A further complication may arise in that the smoke particles may have a size distribution which changes as a function of time. If the particles have different radii, with $N(a)da$ particles with radii between a and $a + da$ per unit volume, then

$$\gamma = \int_0^\infty Q_{\text{ext}} N(a) \pi a^2 da, \quad (33)$$

where Q_{ext} depends upon the argument $x = 2\pi a/l$.

DEVELOPMENT AND ANALYSIS OF THE MODEL

A model has been developed based on the formulae derived above. We will assume

- that the incident light is a plane wave and unpolarized,
- the optical power from the input fiber with a numerical aperture(NA) of 0.3 is 1 mW,
- the wavelength (λ) is 780 nm, and
- the diameter of the circular chamber is 10 cm.

With no smoke present, the power received by the on-axis fiber is calculated to be approximately 0.045 mW [3]. For this model we have assumed that the power radiated by the illuminating fiber is 1mW at 780 nm, such that

$$\begin{aligned}I_0 &= 1 \text{ mW,} \\ \lambda &= 780 \text{ nm, and} \\ k &= 2\pi/\lambda = 8.055 \times 10^6.\end{aligned}$$

For the Mie region, the particle diameter (d) varies as

$$0.1\lambda < d < 4\lambda. \quad (34)$$

Thus the particle size varies from 0.078 μm to 3.12 μm , and the size parameter x ($=2\pi a/\lambda$) varies from 0.157 to 12.56. For heptane the mean diameter is in the range of 0.01 μm to 0.2 μm . The refractive index (m) of heptane is 1.38. The particle size and refractive index are important because i_1 and i_2 are functions of x , m , and q . The imaginary component of m accounts for the amount of light absorbed by the sphere, and this data was not available for heptane. Also, values of i_1 and i_2 for $m=1.38$ were not available. A graph of $I(q)$ for $m=1.33$ and $x=10$ to 18.5 is available in [4], where $I(q) = (i_1+i_2)/2\pi x^2$. This was the closest approximation available for values of i_1 and i_2 for heptane. This graph was digitized, and a sixth degree polynomial curve fit was made to the data. The results showed that this was not a good approximation to the data. A gaussian curve with a standard deviation of 4 and scaled by a factor of 280 was then used to fit the data. Figure 3 whows that the gaussian curve gives a very good fit to the data. This was used in the computer program for the scattered intensity coefficient.

With r being the distance from the center of the sphere and assuming N as unity, the

equation

$$I = N \frac{I_0(i_1 + i_2)}{2k^2 r^2} \quad (35)$$

was implemented.

The intensity of the proceeding beam decreases in a distance l by the fraction e^{-gl} , where g is the extinction coefficient. g was calculated, for $a = 2.29 \mu\text{m}$ and $Q_{\text{ext}} = 2$, to be $3.311225 \cdot 10^{-11}$. This is a very small number and the exponent of such a small number is 1. This can be expected for the values used and the very small distance which is traveled by the beam after interacting with the particles.

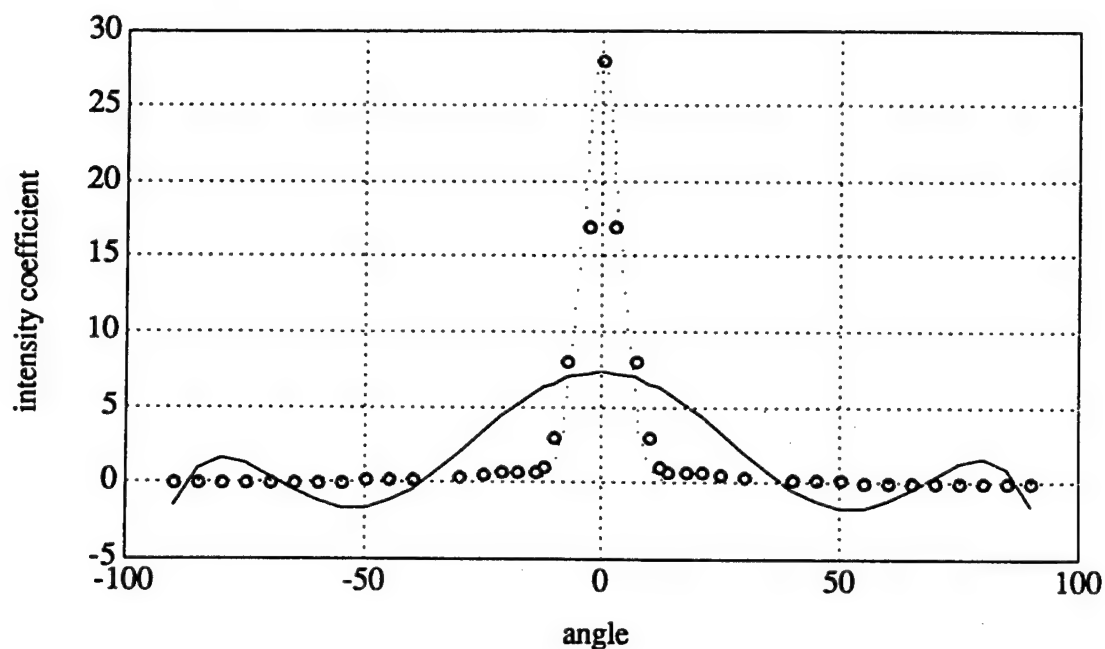


Figure A3- Digitized intensity coefficient $I(q)$ showing the polynomial curve fit (solid line) and the Gaussian curve fit (dotted line) to the data (circles).

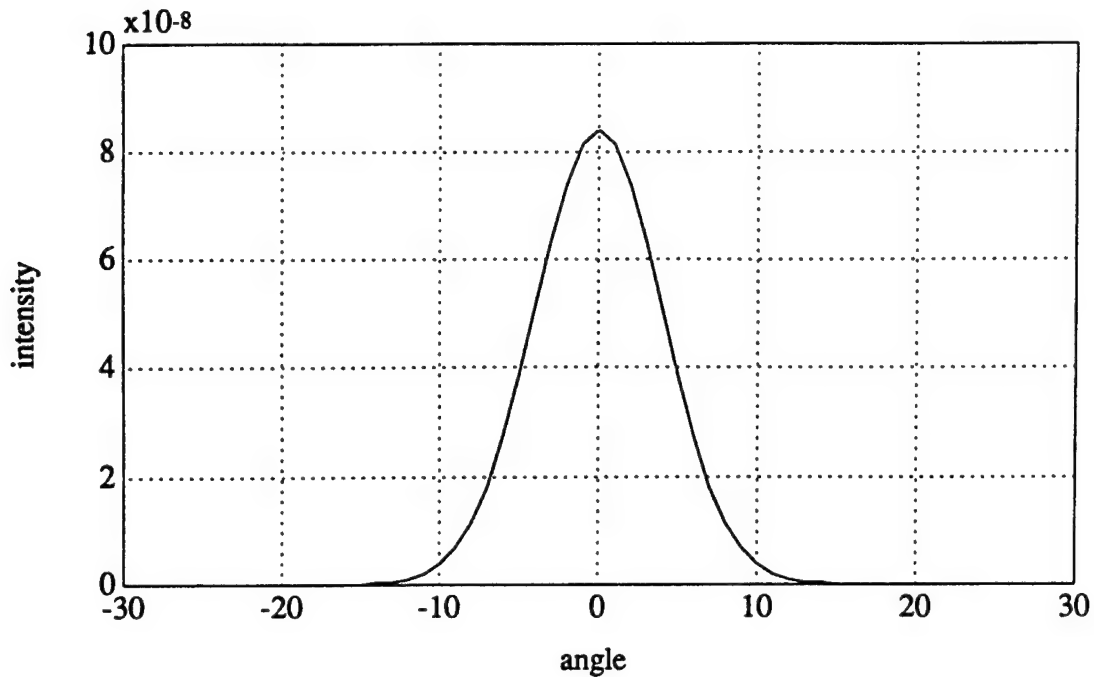


Figure A4- Scattered intensity for a single incident ray

Figure 4 shows the scattered intensity profile (W/m^2) as a function of scattering angle for single ray interacting with a particle. We see that the scattered intensity is very small after 10° . The receiving fiber (with an assumed NA of 0.3) will detect the light from a bundle of rays. It is stated in [4] that the flux scattered is simply the sum of these quantities for all the particles illuminated, provided the subsequent extinction of the scattered light in traveling to the boundary of the particle suspension can be neglected, as is in our case. Since the rays of light diverge from the end of the input fiber, a computer program was developed to shift the intensity profile of the on-axis ray in steps of 1° , for a range of angles varying from -25° to 25° , accounting for all the incident rays within the NA of the input fiber. This was then stored in the form of a matrix for each degree of angle. Then the resultant intensity was obtained by adding the contribution for each ray in the range -25° to 25° .

Figure 5 shows this scattered intensity profile. It is observed that the magnitude of the intensity increases by approximately a factor of 10 and the scattered pattern varies from -12° to 12° . This was anticipated because we have assumed a large particle size, and it is stated [4,5,6] that as the particle size increases the forward scattering lobe becomes narrower. In [4] it is stated that the flux contained in the forward scattering lobe, when the particle diameter exceeds a few microns, is 84% of that geometrically incident on the particle and lies within an angle of about $\pm 35/d$ degrees

(d is the diameter in microns). This gives a forward lobe scattering angle of approximately 15° for our parameters, confirming our results.

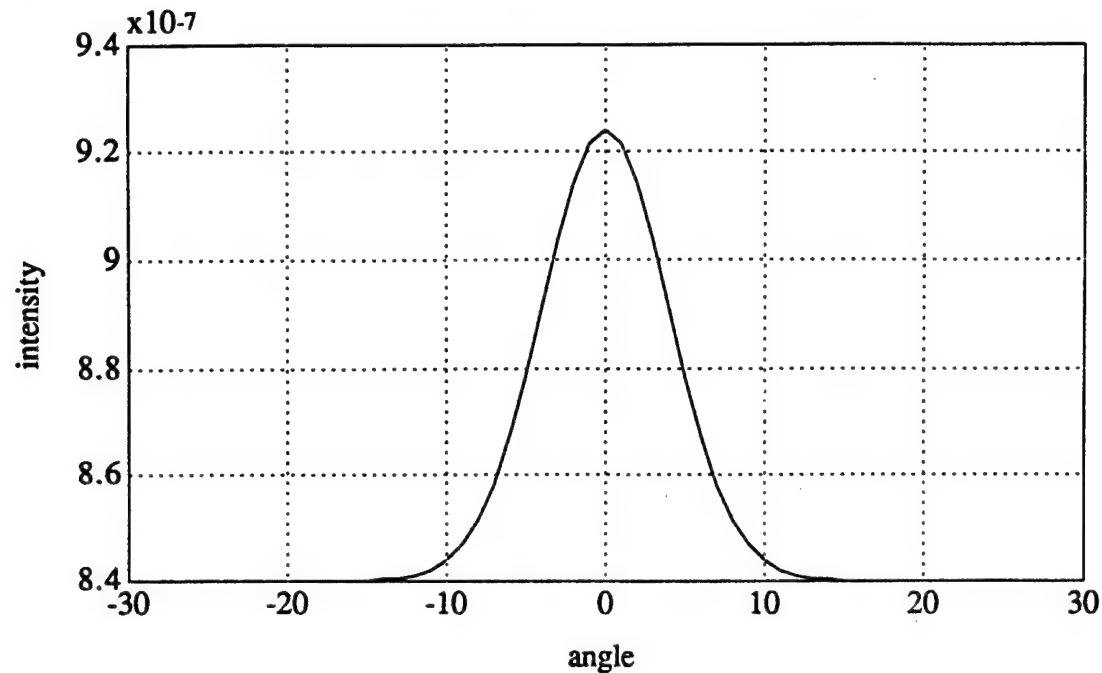


Figure A5- Total scattered intensity for each ray interacting with a smoke particle

In addition, the case for a Gaussian distribution was assumed for the intensity profile of the input fiber. The angular scattering observed was almost the same as for a uniform intensity assumption. Only the magnitude of the intensity distribution changed slightly due to the shape of the Gaussian profile. Figures 6 and 7 show the corresponding cases for the Gaussian distribution.

Thus, a multimode fiber with a NA of 0.3 would be a good choice for the input, on-axis and off-axis fibers. Since the size of the smoke detector is small and the scattering is less for small distances the use of collimating lenses is not necessary. The placing of the off-axis fiber can be customized for the smoke generated by each environment, by setting the parameters in the program and observing the output scattering profile. Then based on the sensitivity of the detector used, the off-axis fiber can be optimally placed. Also, based on the detector sensitivity, an electronic circuit can be used to control the

threshold of the detector. By doing so, the off-axis fiber can be placed at a certain fixed angle from the on-axis fiber, and its sensitivity to detect a particular type of smoke can be controlled by setting the detector threshold

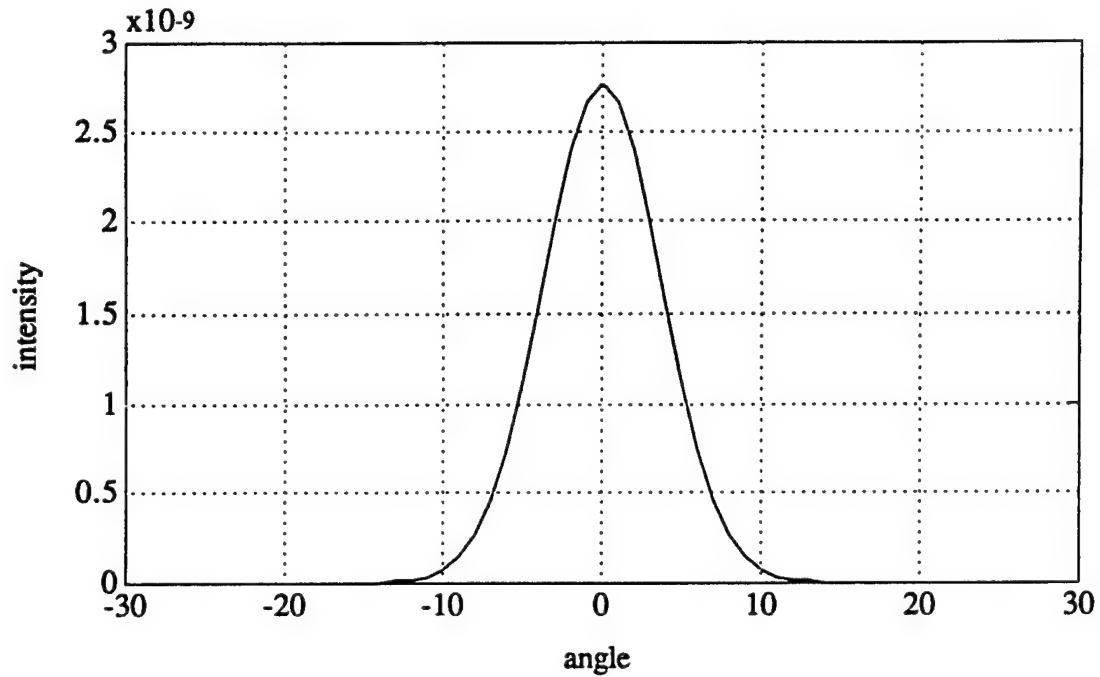


Figure A6- Scattered intensity for a single, gaussian distributed, incident ray.

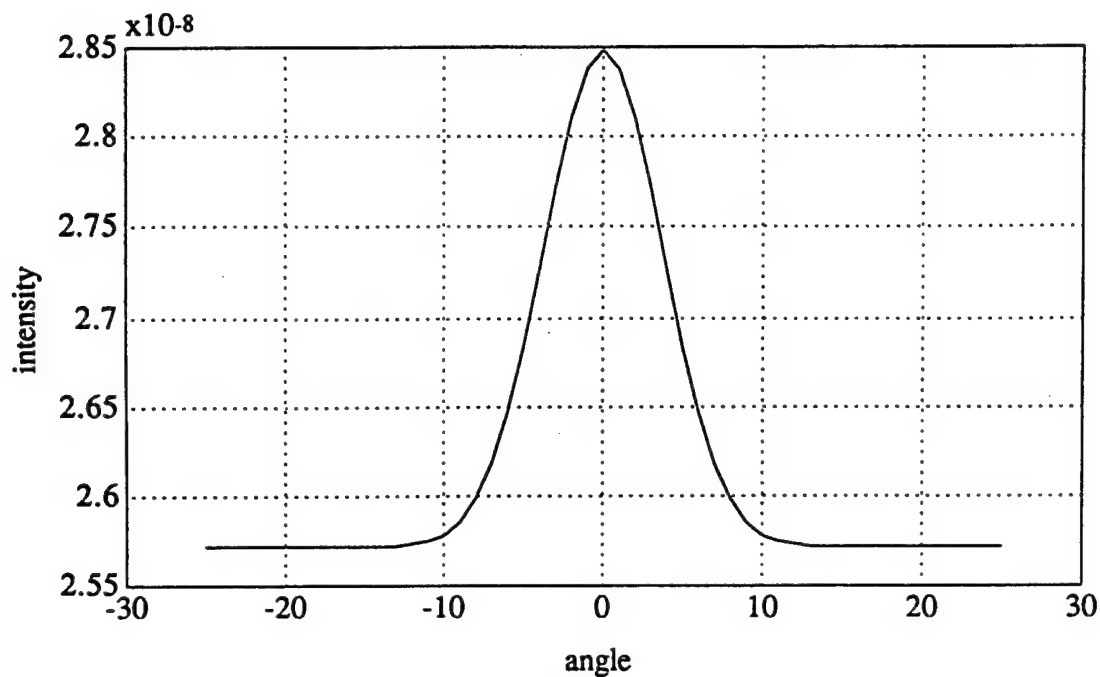


Figure A7-Total scattered intensity for each gaussian distributed ray interacting with a smoke particle.

REFERENCES

- [1] T. G. K. Lee, G. Mulholland, "Physical properties of smoke pertinent to smoke detector technology," NIST, *publication NBSIR 77-1312, National Bureau of Standard*, Nov 1977.
- [2] "Smoke detector design and smoke properties," *NBS Technical Note 973*, Nov 1978.
- [3] D. Marcuse, "*Optical fiber measurements*," McGraw-Hill, 1984.
- [4] C. N. Davies, "*Aerosol Science*," Academic Press, 1966.
- [5] H. C. Van de Hulst, "*Light Scattering by Small Particles*," John Wiley and Sons, 1957.

- [6] M. Kerker, "*Electromagnetic Scattering*," Pergamon Press, 1963
- [7] J. V. Dave, "Scattering of Electromagnetic Radiation by a Large, Absorbing Sphere," *IBM Journal of Research and Development*, Vol. 13(3), pp.302-313, May 1969.
- [8] G. C. Stokes, *Tran. Camb. Phil. Soc.* 9, 399, 1852

APPENDIX B - OPTICAL FIBER SMOKE SENSOR TESTS ON EX-USS SHADWELL

Optical fiber smoke sensors of the spectrometric type were tested on the ex-USS SHADWELL to confirm operation in the shipboard environment in real fire conditions. The tests were successful. Fire testing of the optical fiber smoke sensors was completed during April/May 1993 and Sept 1993 on decks 2 and 3 of the SHADWELL as shown in Figures B1 and B2. Class A fires were lit in Berthing 2 of the third deck with both alcohol and wood, sufficient to generate great quantities of smoke and temperatures of several hundred degrees Centigrade. As the fires progressed, the heat and smoke rose to the second deck, first into Berthing 1 and then outward into the adjoining passageways, depending on which hatch and doors were open at the time.

During each test the optical fiber smoke sensors were mounted in the passageway immediately starboard of Berthing 1. During the April/May tests, the smoke sensor was located at 2-15-3, 90 inches above the deck and surrounded by ducting and cable runs. During the Sept tests, the smoke sensors were located at 2-18-3 at 60 inches and 120 inches above the deck; they were physically mounted on the forward end of optical density meters resident on the SHADWELL.

In both tests, the outputs of the optical fiber smoke sensors was compared with optical density meters resident on the SHADWELL. The resident optical density meters operate at a wavelength of 830 nanometers and use optical power absorption over a 1 meter path length as an indication of obscuration. Operation is checked by setting the optical power received at 0% for a clear atmosphere and then setting the reading to 100% obscuration when the light path is completely blocked. The lens are cleaned after every test.

The optical fiber smoke sensor tested on the ex-USS SHADWELL was selected from several types of possible sensors, investigated during this program. Bench top models of the optical fiber smoke sensors were constructed for obscuration, scattering, and spectrometric types of sensors. Laboratory experiments showed that the spectrometric type was the best selection based on performance, availability of parts to meet the evaluation schedule, and commonality of opto-electronics package with other damage control monitoring sensors. (This does not necessarily mean the spectrometric smoke sensor should be the type selected for 6.3 development. The scattering optical fiber smoke sensor is a strong candidate also.) The spectrometric optical fiber smoke sensor was checked for proper operation in a standard smoke chamber designed according to Underwriters Laboratories standards. Patents have been submitted on both the scattering and spectrometric smoke sensors.

The spectrometric optical fiber smoke sensor is shown mounted on the ex-USS SHADWELL in Figure B3. It is a reflective configuration with a 2 inch air path, 4 inch round trip. The opto-electronics package is shown in Figure B4 and is the identical type of package used in earlier optical fiber temperature tests on the SHADWELL; this package was left on the SHADWELL from April until Sept of 1993 and operated continuously during the hot and humid Alabama summer.

Figures B5 through B8 are selected samples of the optical fiber smoke sensor evaluation results. In each case the data recorded from the fiber sensor is plotted on the same graph as the data recorded for the optical density meter resident on the SHADWELL.





FILE: JLS20 DATE: 10/5/93
 DSK: 2 TEST: FDE 93

KEY
 Fire plug
 Electrical outlet
 Saddle
 Water tight hatch

OC Office
 OC Aft
 Berthing 1
 New SMS Console
 Repair 2
 2-9-1-Q

2-26-2
 2-27-2
 2-28-2
 2-29-2
 2-30-2
 2-31-2
 2-32-2
 2-33-2
 2-34-2
 2-35-2
 2-36-2
 2-37-2
 2-38-2
 2-39-2
 2-40-2
 2-41-2
 2-42-2
 2-43-2
 2-44-2
 2-45-2
 2-46-2
 2-47-2
 2-48-2
 2-49-2
 2-50-2
 2-51-2
 2-52-2
 2-53-2
 2-54-2
 2-55-2
 2-56-2
 2-57-2
 2-58-2
 2-59-2
 2-60-2
 2-61-2
 2-62-2
 2-63-2
 2-64-2
 2-65-2
 2-66-2
 2-67-2
 2-68-2
 2-69-2
 2-70-2
 2-71-2
 2-72-2
 2-73-2
 2-74-2
 2-75-2
 2-76-2
 2-77-2
 2-78-2
 2-79-2
 2-80-2
 2-81-2
 2-82-2
 2-83-2
 2-84-2
 2-85-2
 2-86-2
 2-87-2
 2-88-2
 2-89-2
 2-90-2
 2-91-2
 2-92-2
 2-93-2
 2-94-2
 2-95-2
 2-96-2
 2-97-2
 2-98-2
 2-99-2
 2-100-2

KEY

-  Fire plug
-  Electrical outlet
-  Sawtooth
-  Water light hatch

29 28 27 26 25 24 23 22 21 20 19 18 17 16 15 14 13 12 11 10 9

Figure B2 - Third Deck Plan View, Ex-USS SHADWELL.

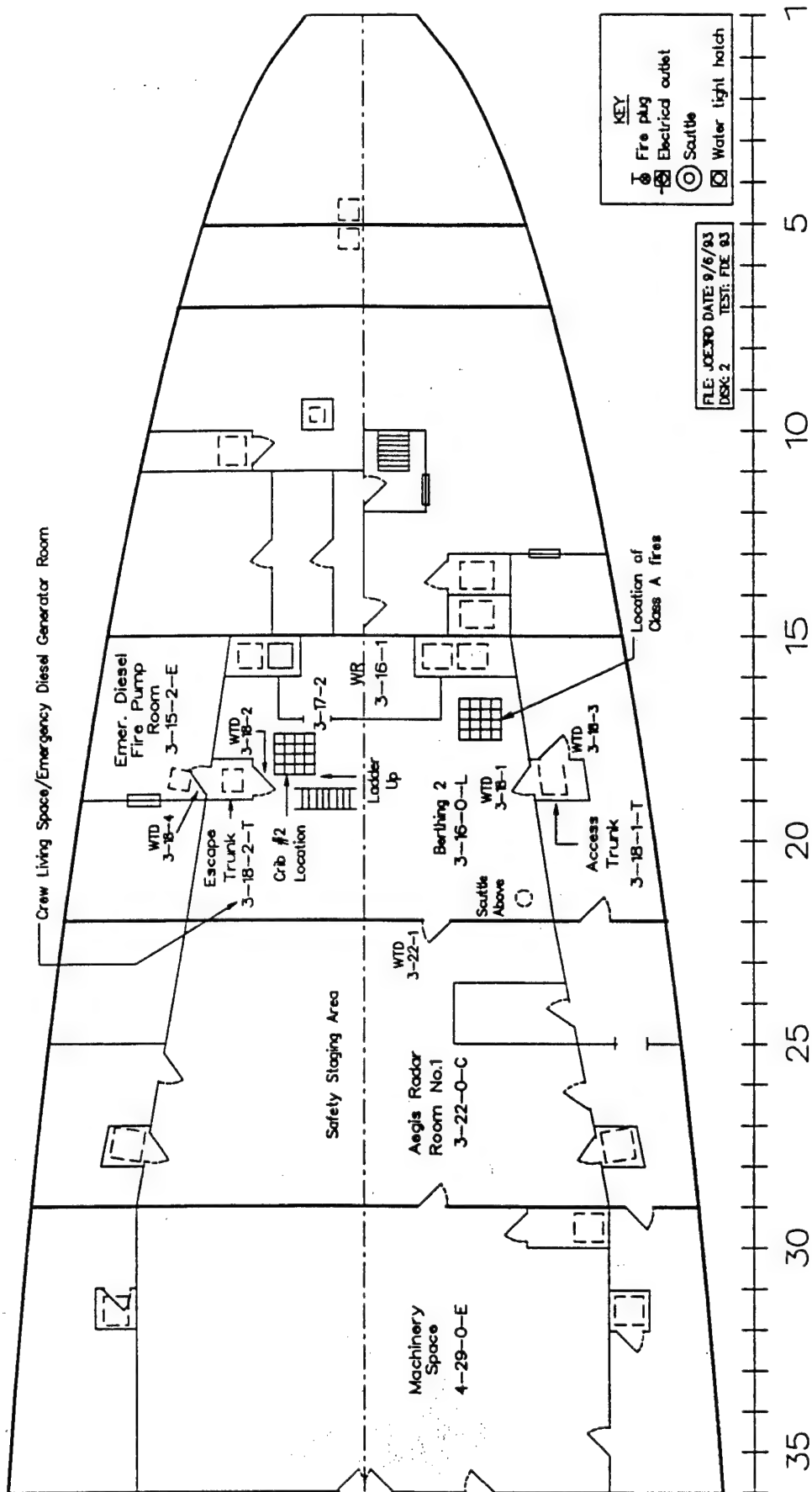


Figure B3 - Spectrometric Optical Fiber Smoke Sensor Element.

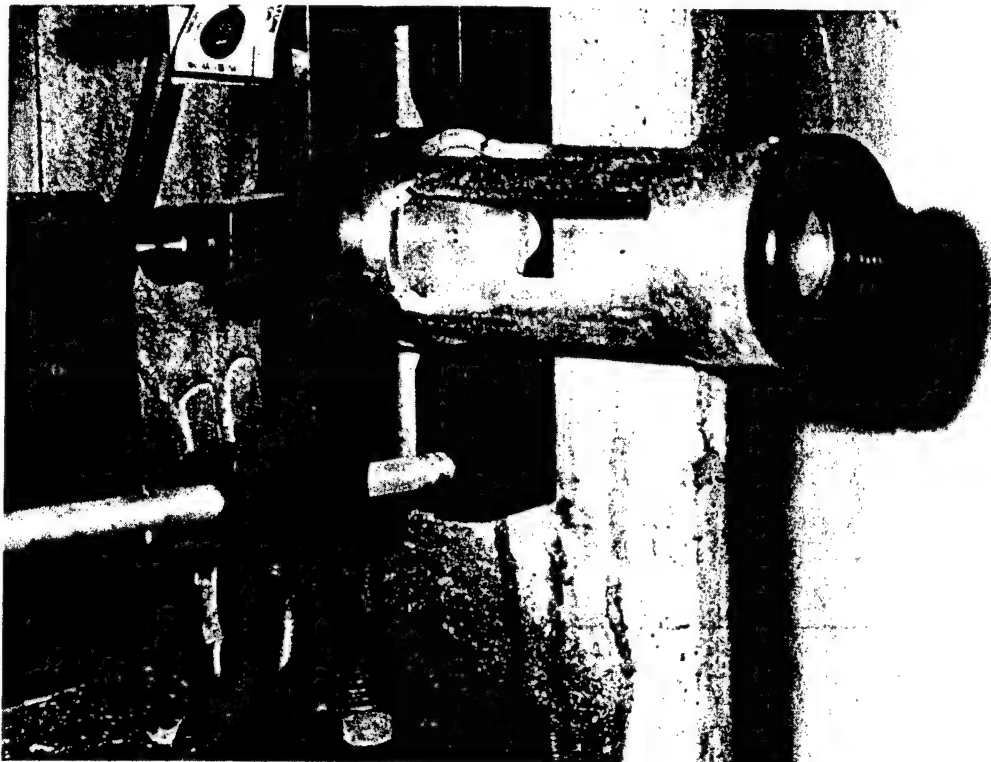


Figure B4 - Spectrometric Optical Fiber Smoke Sensor Opto-electronics Package.

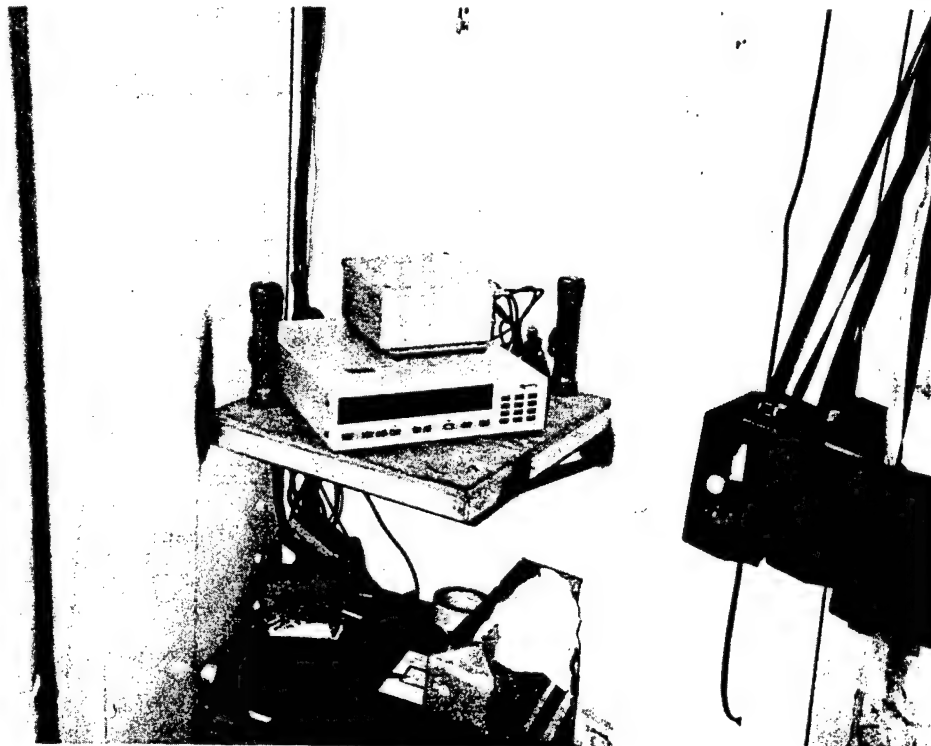


Figure B5 - Optical Fiber Smoke Sensor Test Results
Ex-USS SHADWELL Fire Test FD-F19 Sept 1993

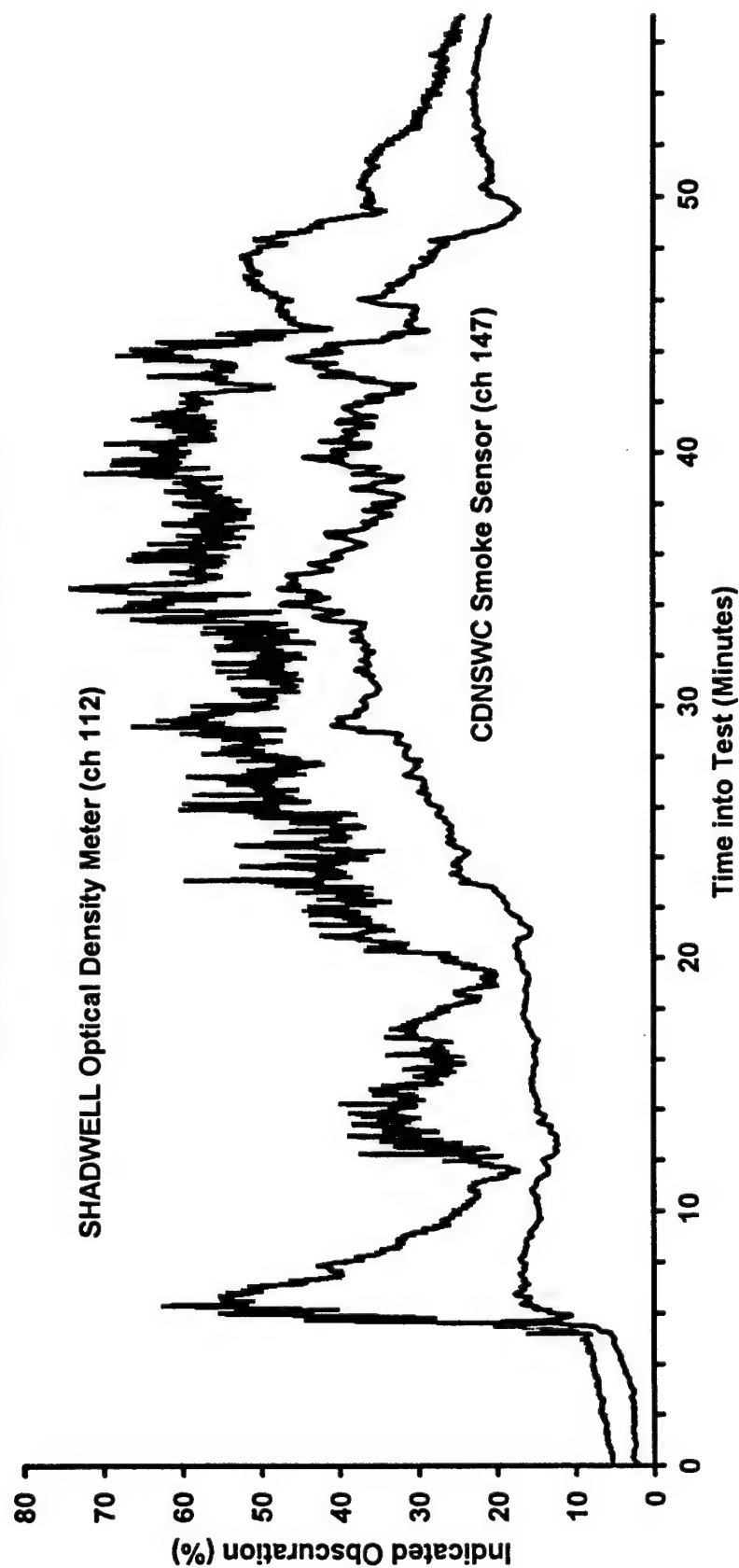


Figure B6 - Optical Fiber Smoke Sensor Test Results
Ex-USS SHADWELL Fire Test FD-D1 Sept 1993

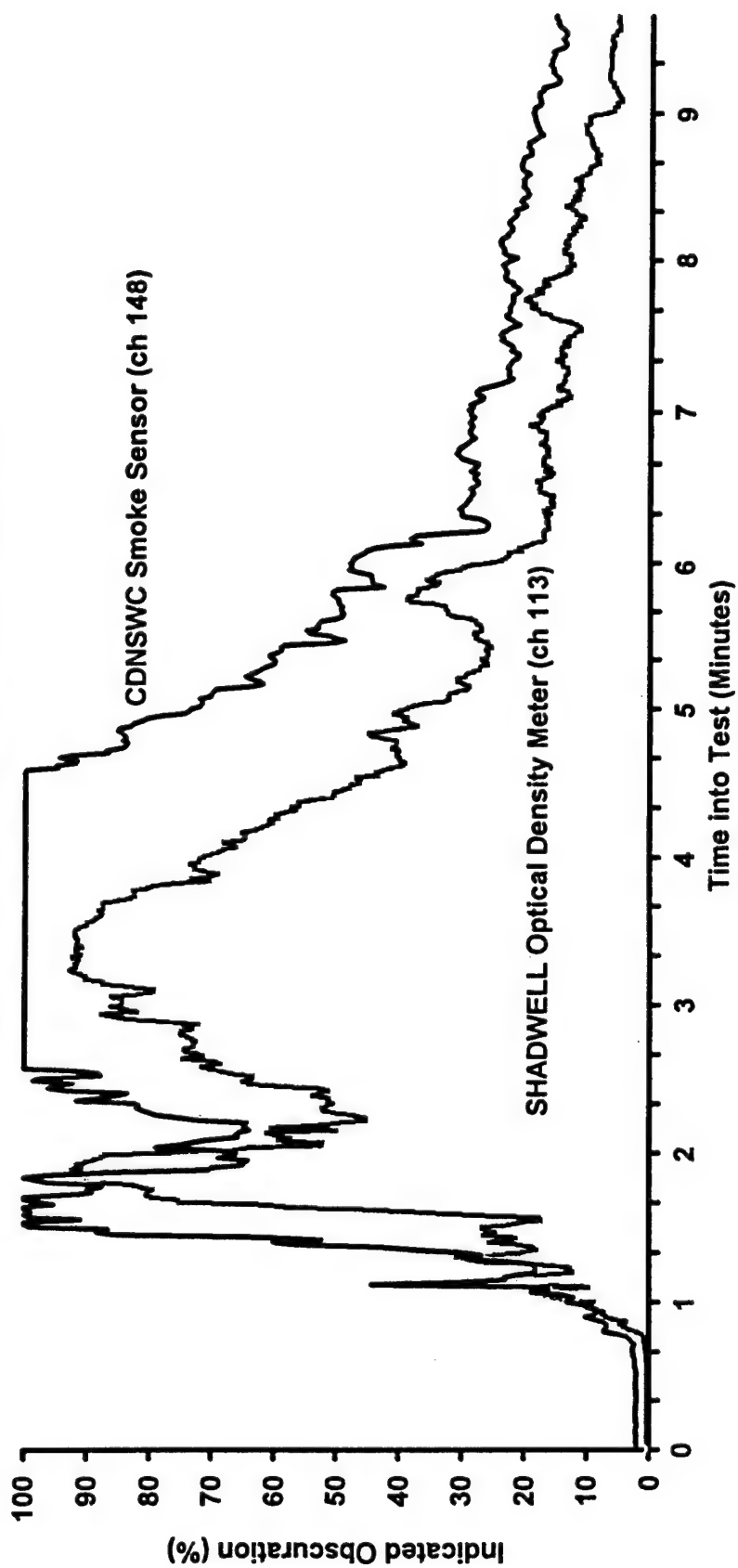


Figure B7 - Optical Fiber Smoke Sensor Test Results
Ex-USS SHADWELL Fire Test FD-F7 May 1993

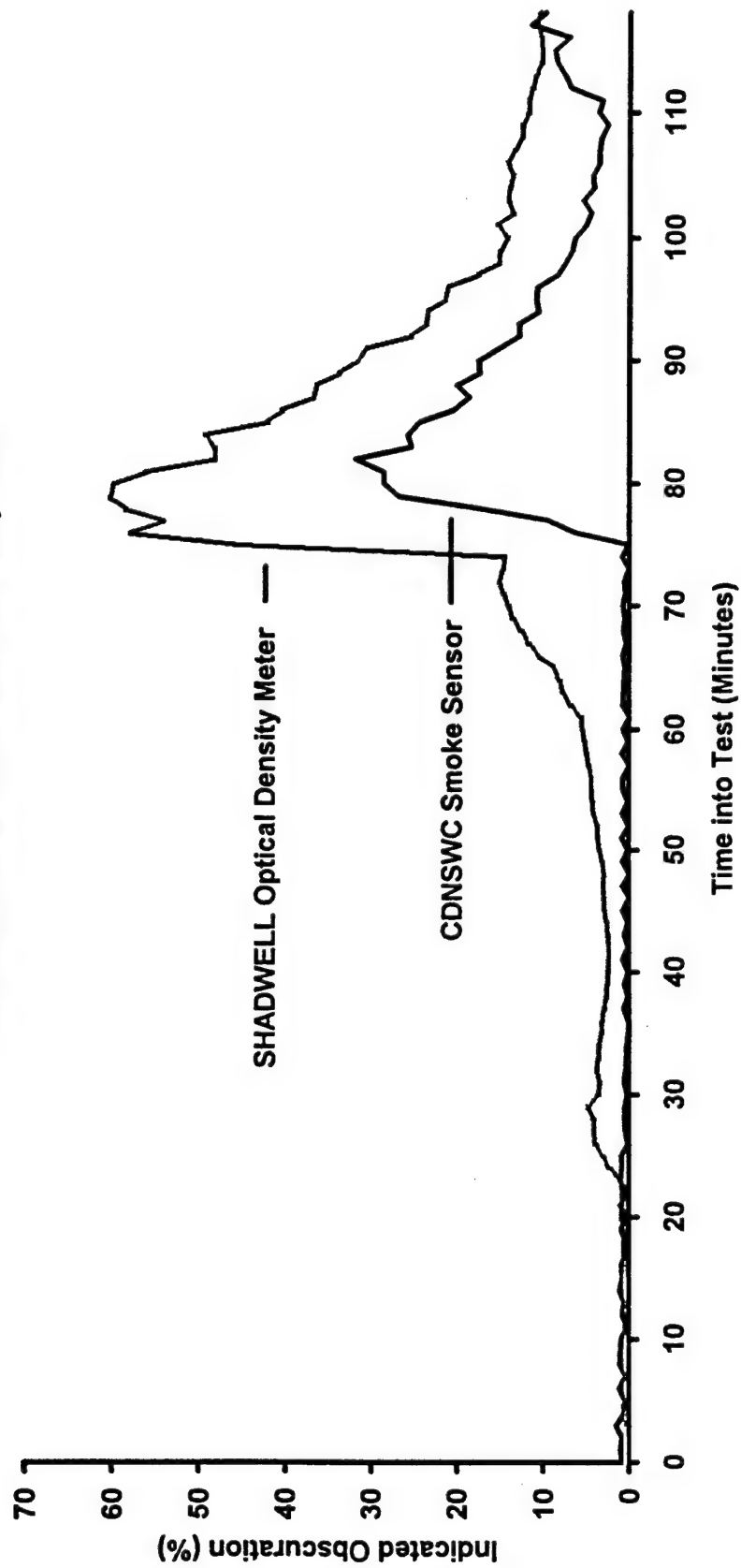
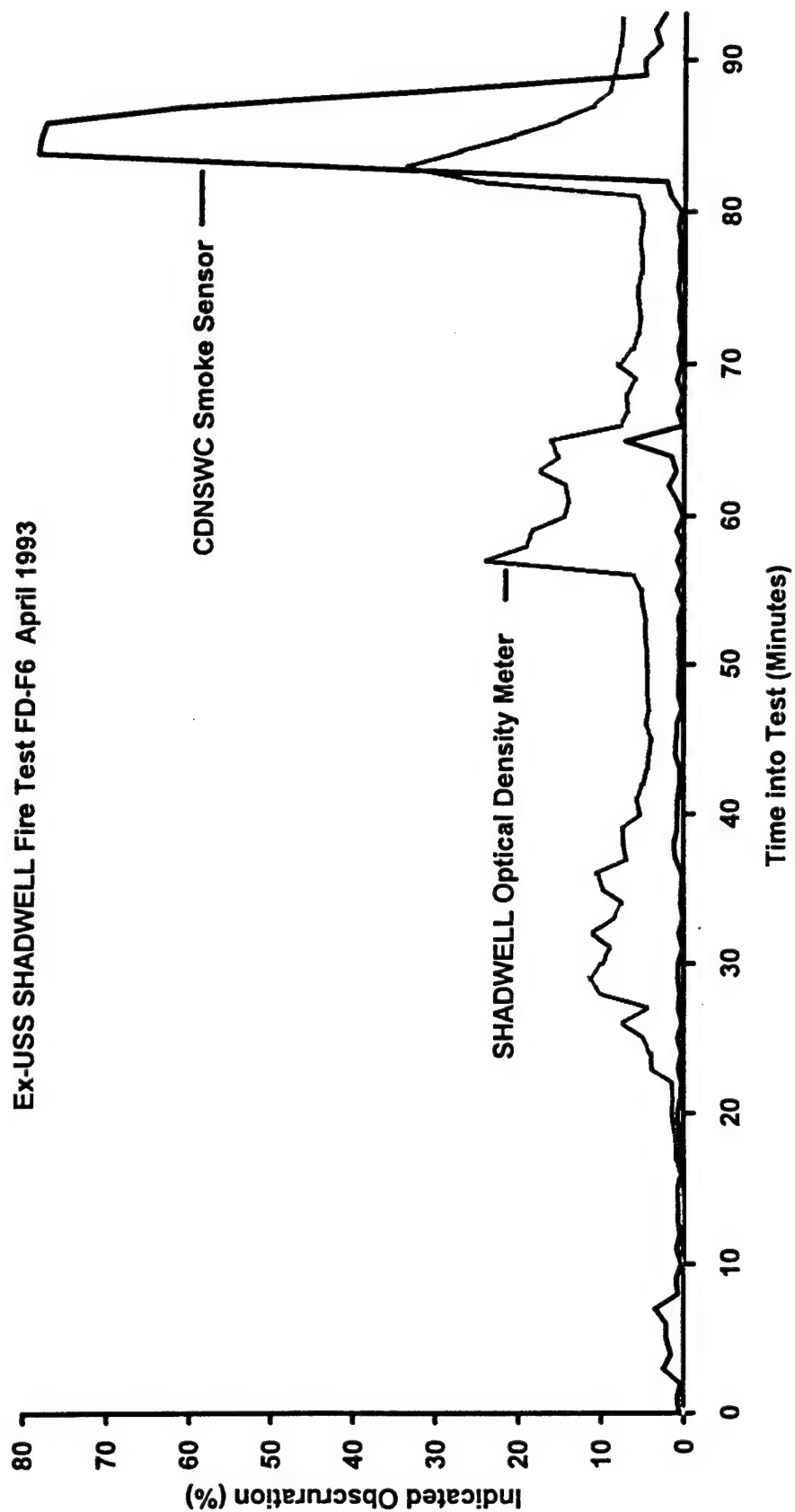


Figure B8 - Optical Fiber Smoke Sensor Test Results
Ex-USS SHADWELL Fire Test FD-F6 April 1993



Sampling path lengths of the optical fiber sensor and the resident SHADWELL optical density meter were 4 inches and 40 inches, respectively. This explains some of the differences observed in the recorded data but the major difference arises from the uncalibrated state of the optical fiber smoke sensor. Variable air currents in the passageway also caused different indications of the smoke density for the two kinds of sensors. In all graphs, the two sensors agree in form. This accomplished the objective of the evaluation which was to demonstrate operability of the optical fiber smoke sensor in the shipboard environment.

Figure B5 shows test results of one of the Sept 1993 fires tests for the spectrometric optical fiber smoke sensor. The fiber sensor is plotted as channel 147 and the SHADWELL optical density meter is plotted as channel 112.

For smoke detectors, it is standard operating procedure to calibrate or check operation with artificial smoke generators. This was done during the Sept 1993 tests on the ex-USS SHADWELL with results shown in Figure B6. Channel 148 is the optical fiber smoke sensor data and Channel 113 is the SHADWELL optical density meter. Again the two sensors agreed in form.

Figures B7 and B8 show test results from the 2 tests in April/May 1993. Results from each sensor were similar in variation but not in absolute in amplitude.

The data shown in Figures B5 through B8 are typical of the results obtained during the smoke sensor evaluation on the SHADWELL. However, we found some notable problems some of which were fixed in our laboratory and some of which were left for solution in a follow on development program.

During one of the tests, there was a differential expansion in the smoke sensor due to rise in temperature and the sensor exhibited a high error with changing temperature. This temperature error was found to be a function of materials used in the sensor construction and the quality of the alignment of the optical components; a good optical design and alignment greatly reduces the temperature coefficient by gathering all the light into receiver with some tolerance for movement in the optical beam while being heated and cooled. Figure B9 is a graph of data from a laboratory test for a smoke sensor design completed after the SHADWELL test; the results demonstrate operation with sufficiently low temperature coefficient over the temperature range of 0°C (32°F) to 100°C (212°F).

Another problem was caused by water coatings on the lens and high humidity in the sampling chamber. Evidence was inconclusive during the SHADWELL evaluation as some tests showed relative immunity to the effects of water coating on the lens while others showed errors outside the allowable performance goals. Figure B10 is a graph of data from laboratory tests on a smoke sensor design completed after the SHADWELL test; error remains within acceptable limits for all values of relative humidity below 95%. There is reason for optimism for designing an optical fiber smoke sensor that is immune to water coatings on the optical surfaces; if this is achievable, it would represent a significant performance advantage for the spectrometric optical fiber smoke sensor. The theoretical basis for lens water coating not affecting the indicated smoke obscuration depends on the fact that in the processing, a ratio is formed of the power of two optical wavelength regions, creating compensation for broadband variation of the received optical power.

Figure B9 - Optical Fiber Smoke Sensor
Temperature Test @ 30 Percent Relative Humidity 08 Nov 93

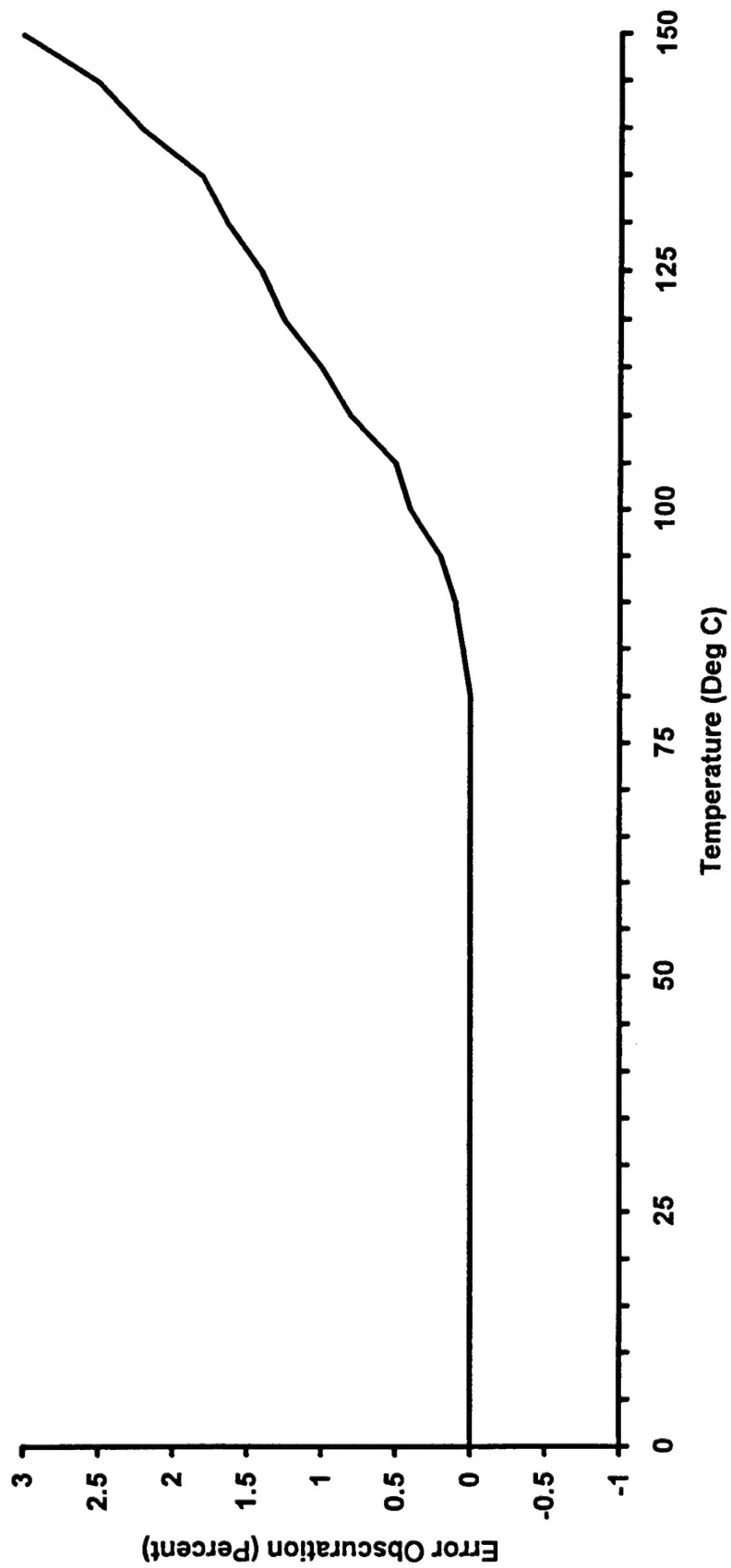
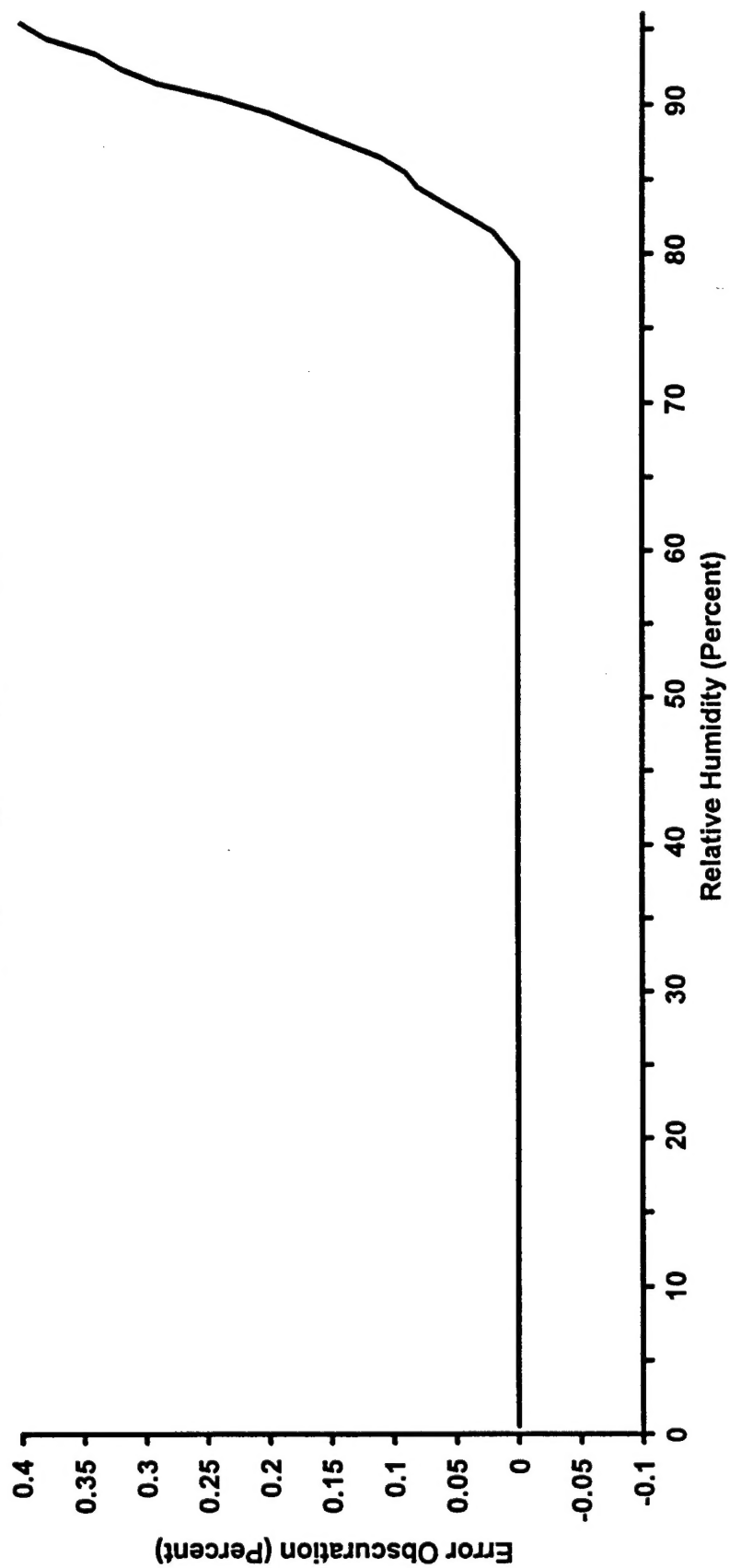


Figure B10 - Optical Fiber Smoke Sensor
Humidity Test @ 30 Degrees C 09 Nov 1993



INITIAL DISTRIBUTION

| Copies | Code | Name |
|--------|-----------|----------------|
| 1 | ONR 33 | J. Gagorik |
| 1 | OPNAV N86 | C. Bogner |
| 14 | NRL | |
| 1 | 252 | R. Holland |
| 1 | 5600 | T. Giallorenzi |
| 1 | 5603 | G. Cogdell |
| 10 | 6183 | P. Tatem |
| 1 | 6183 | F. Williams |

21 NAVSEA

| | | |
|---|-------|-----------------|
| 1 | 03EIR | D. Yee |
| 1 | 03G | Cdr. J. Flood |
| 1 | 03G | Cdr. R. Mott |
| 1 | 03G1 | W. Davison |
| 1 | 03G22 | D. Kay |
| 1 | 03G3 | H. Kuzma |
| 1 | 03JB | J. Moschopoulos |
| 1 | 03J1 | T. Dameron |
| 2 | 03J4 | G. Theisz |
| 1 | 03J4 | F. Leland |
| 1 | 03K32 | G. Miller |
| 1 | 03K32 | C. Mai |
| 1 | 03K12 | L. Blackwell |
| 2 | 03K31 | C. Jacobson |
| 1 | 03K31 | C. Trude |
| 1 | 03R1 | J. Tobin |
| 1 | 03R1 | A. Smookler |
| 1 | 03R1 | B. Smale |
| 1 | 04DS | J. Dressel |

4 NIST

| | | |
|---|--------|-----------------|
| 1 | | G. Muholland |
| 1 | | W. Grosshandler |
| 1 | 814.02 | G. Day |
| 1 | 814.02 | A. Rose |

2 NSW, Dahlgren Div

| | | |
|---|-----|------------|
| 1 | N35 | D. Knudsen |
| 1 | N35 | G. Brown |

1 NCCOSC 821 R. Kochanski

| Copies | Code | Name |
|--------|----------------|----------------|
| 2 | MSD/NWAC | |
| 1 | MS-30A | P. Strucker |
| 1 | MS-31C | W. Hamann |
| 1 | SWOS | Cdr. J. Farley |
| 2 | Virginia Tech, | R. Claus |
| 2 | ECO, Inc. | M. Ransford |
| 1 | Hughs Assoc | J. Sheffey |

CARDEROCKDIV, NSW, DISTRIBUTION

Copies Code Name

| | | |
|----|------|--------------|
| 1 | 0113 | D. Winegrad |
| 1 | 0115 | I. Caplan |
| 1 | 0116 | R. Brengs |
| 1 | 201 | D. Sheridan |
| 1 | 2215 | S. Cohen |
| 1 | 3412 | W. Rice |
| 1 | 3421 | TIC (C) |
| 1 | 3422 | TIC (A) |
| 1 | 625 | J. Callahan |
| 1 | 6254 | A. Peters |
| 1 | 6254 | S. Tweedie |
| 1 | 633 | R. Carey |
| 1 | 80 | L. Argiro |
| 1 | 825 | D. Kover |
| 1 | 85 | G. Garduno |
| 1 | 853 | D. Kocsik |
| 1 | 853 | J. Overby |
| 1 | 853 | E. Petrisko |
| 15 | 853 | H. Whitesel |
| 1 | 853 | E. Zivi |
| 1 | 953 | F. Walicki |
| 1 | 9532 | C. Savage |
| 1 | 9532 | N. Albor |
| 1 | 9533 | J. DiTaranto |
| 1 | 9533 | A. Price |